# Transient Photoreceptor Phototropism in Developing Mouse Retina

BY

VITTORIA MANEO
Bachelor Degree, Politecnico di Milano, Milan, Italy, 2016

THESIS

Submitted as partial fulfillment of the requirements
for the degree of Master of Science Bioengineering
in the Graduate College of the
University of Illinois at Chicago, 2019

Chicago, Illinois

Defense Committee:

Xincheng Yao, Chair and Advisor
James Lee
Enrico Caiani, Politecnico di Milano

## ACKNOWLEDGMENTS

I want to thank everyone that was involved in this work, either physically or with moral support. First of all, I want to thank Dr. Yao and all the people that work in his lab, especially Yiming, who helped me out many times during my experience there. Then, I want to thank my family, that allowed me to travel and study here at UIC. Also, Lynn and Professor Caiani, who helped me when I needed a push to conclude this work. I need to thank all the Italian people that joined the program with me, especially my roommates, who made me laugh and get past all the difficulties that I encountered during this experience. Last but not least, I want to thank my boyfriend Vasco, whose support is always fundamental.

VM

# TABLE OF CONTENTS

## LIST OF TABLES

# LIST OF FIGURES

## LIST OF FIGURES (continued)

## LIST OF ABBREVIATIONS

| | |
|---|---|
| TRP | Transient Retinal Phototropism |
| ROS | Rod Outer Segments |
| SCE | Stiles-Crawford Effect |
| NIR | Near-Infrared |

## SUMMARY

This work focuses on quantifying the response of mouse rod photoreceptors to a light stimulus during developmental ages. The purpose is to have a better comprehension of the physiological mechanisms underlying transient retinal phototropism. The three considered post-natal ages are 15, 17 and 19. During this period the increase of ROS length and rhodopsin concentration reaches its peak thus, I expected to see an associated increase in the amplitude of the phototropism elicited by the light stimulus. In particular, rhodopsin is suspected to be a key molecule as far as concern this phenomenon but its role is still unclear.

The observation of mouse rod photoreceptors was achieved with Near-Infrared light microscopy, which allowed to have a clear image of the freshly isolated mouse retinae. The images where acquired at 100 fps and they showed a visible movement in response to the light stimulus.

The results of the data analysis showed that the amplitude of the movement had a sharp increase between 15 and 17 PN days, while the difference between 17 and 19 PN days was statistically irrelevant. This results were consistent with expectations, as the peak of the growth of ROS has a sharper rise during the first two considered ages. The almost indistinguishable difference between 17 and 19 PN days may depend on the fact that the variables are already saturating to the adult value.

# CHAPTER 1

# INTRODUCTION

In 1933 Stiles and Crawford discovered, through psycho-physical studies, that the luminous efficiency of a light ray entering the retina depends on the distance between the ray and the center of the pupil [6]. A light beam entering through the center of the pupil is perceived as brighter than a parallel ray entering from a more peripheral position. This phenomenon, called Stiles-Crawford effect, has been assessed in photopic vision but it is completely absent when the experiment is performed under scotopic conditions [7]. For many years, the causes of this behaviour remained unclear. More recent studies (2013) finally revealed that rod cells respond to the light stimulus with a quick shift towards the light source [8]. This response is too fast to be detected with psycho-physical experiments hence, phototropism could explain why SCE only affects cone photoreceptors.

Photoreceptors phototropism has been extensively studied in frog and it has also been assessed in mouse retinae. The former are favored because of the significantly larger photoreceptors, which allow a better observation and evaluation of the phenomenon. Following studies revealed more features about the response of the rod cells to light stimulation. The physiological causes of TRP however, remain unclear and this study aims to make a step forward in understanding the biomechanics behind the movement of rod photoreceptors. The experiments were performed at three different post-natal ages (15, 17 and 19) on freshly isolated mouse retinae. This ages are critical for the developing of the retina and in particular for ROS. The

photoreceptors were observed through near-infrared light microscopy, which has been used in all the previous studies and allowed a clear observation of the phenomenon. The use of mammals instead of amphibians allows a closer comparison with the human retina. This study focuses on the possible role of rhodopsin, the visual pigment responsible for vision in rod cells. Rhodopsin is a key element in ROS; this molecule has already been connected to the growth of ROS itself [9] and it could have a major role in phototropism.

Rod photoreceptors are more fragile than cones and they are the first to die when it comes to age-related macular degeneration [10]. Moreover, rhodopsin, which is the photopigment contained in rod photoreceptors, is particularly sensitive to mutations [11; 12]. In many cases, a mutation leads to the progressive death of photoreceptor cells. As the photoreceptors die, the visual acuity of the patient decreases and eventually, it will lead to complete blindness. An early detection of these conditions is crucial. A more extensive comprehension of TRP could lead to a significant noninvasive biomarker for the early detection of retinal degeneration related to rod photoreceptors.

# CHAPTER 2

# PREVIOUS WORK

## 2.1 Rods characteristics

The retina is a complex structure lying in the back of the eye that converts light stimuli into images, allowing vision. Photoreceptor cells are the ones responsible for this conversion as they transform photons into an electrical signal. There are two types of photoreceptors, cones and rods. The former are responsible for vision during day-time, while the latter have a higher sensitivity which makes them useful for night-time vision [1].

In mouse retina, the majority of the photoreceptors is represented by rods (about 97%), which are responsible for scotopic vision [13]. The dominant presence of rods allows to focus on their contribution to phototropism and to neglect the presence of cones. Like cone cells, rods are constituted by four different sections: outer segment, inner segment, cell body and synaptic terminal. The first one is the one responsible for phototropism and this is why we will focus only on the outer segment of the photoreceptors.

ROS are constituted by a dense stack of membranous disks (approximately 500-2000 disks) with a diameter of $1.2\mu m$ and a total length of about $24\mu m$ at the adult age, while the space between the disks is about $28nm$. A relevant feature is that the disks are completely separated from the plasma membrane (differently from cones), so they can be considered discrete units.

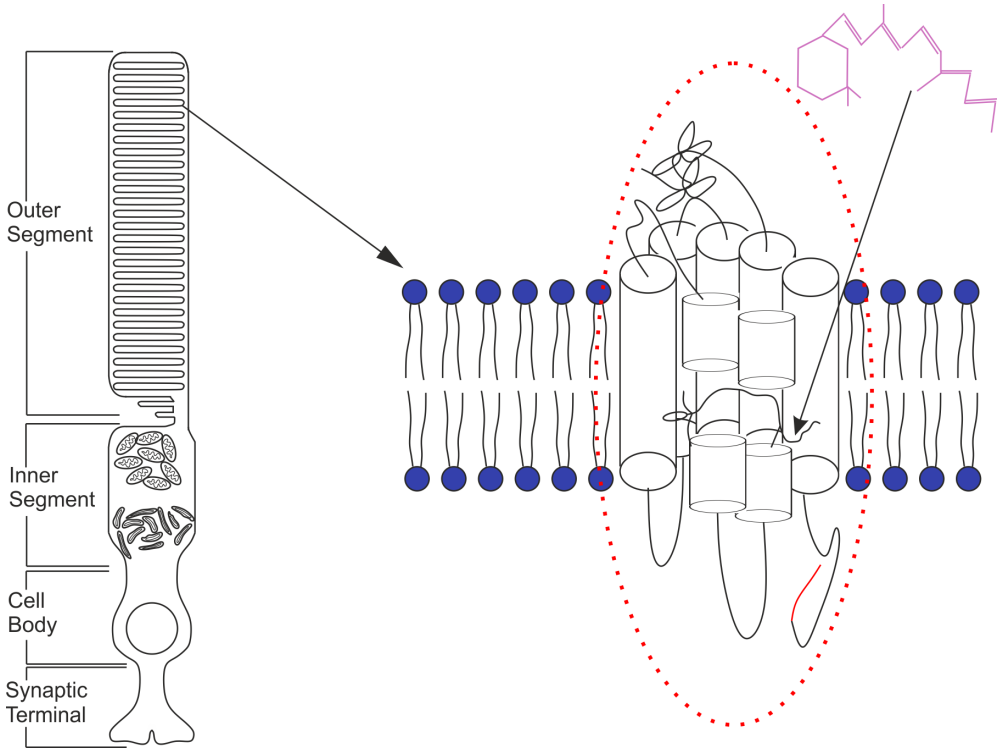


Figure 1: Rod and rhodopsin schematic structure. Image adapted from [1]

ROS contains the visual pigment that allows vision, rhodopsin. This photosensitive molecule is embedded in the disks membrane and its high concentration is responsible for the sensitivity of rods. Rhodopsin is made of two components: opsin and retinal. Opsin is a G protein-coupled receptor and it is sensitive to light; it is made of seven alpha-helices that are embedded in the double-lipid membrane of the disks. The seven portions of the opsin surround the retinal, which lies horizontally inside the membrane. Retinal is a form of vitamin A and it is a photo-reactive chromophore. You can observe the structure of rod and rhodopsin in Figure 1.

When rhodopsin is hit by light, it bleaches and causes the phototransduction cascade that allows vision. When a photon is absorbed by the retinal chromophore, it isomerizes from the 11-cis to the all-trans form. The photo-isomerization of the retinal, elicits the bleaching of the opsin molecule. The absorbance spectra are determined by the opsin molecule and its interaction with the retinal chromophore, the opsin in rod photoreceptors strongly absorbs the green-blue light. Opsin molecules respond by changing their structure and eventually becoming Metarhodopsin II, which is an unstable form and so the opsin and the all-trans retinal separates from each other. The opsin activates the protein transducin, which in turn activates PDE (phosphodiesterase). PDE hydrolyzes cGMP into 5-GMP, causing the closure of the cGMP gated sodium channels. The sodium channels where responsible for the depolarization of the cell (-40mV) and as they close, the outgoing flux of potassium causes the hyperpolarization of the cell. The voltage-gated calcium channels close and this reduces the concentration of calcium inside the cell. The reduced amount of calcium is mirrored by a reduction in the releasing rate of glutamate neurotransmitter which ultimately leads to a reduced current to the brain [14].

Rods are highly sensitive to light, they can be activated even by a single photon. The wavelength sensitivity for mouse rod photoreceptors is reached around $500nm$ (green-blue) and they become insensitive for wavelengths higher than 640 $nm$ (red). This means that green light is suited for eliciting a response of the photoreceptors [15].

## 2.2 ROS development

In order to explain the behavior of the photoreceptors upon light stimulation, it is necessary to understand how ROS change during the same age period. The disks in ROS are continually

renewed, even once the adult length is reached. They are synthesized at the base of the outer segment and then, they are disposed by the RPE (retinal pigmented epithelium) once they reach the apex [16; 17]. During developmental ages, this process favors the synthesis of new disks with a lower disposal rate and this allows the growth (in length) of ROS. According to the studies of Matthew La Vail [5], the rate of synthesis of ROS in the mouse retina is maximal between 13-17 PN days (about 120 disks per day, 1.6 times greater than the adult rate), while the disposal rate of the disks is only 70% of the adult value. Consequentially, the length of ROS increases linearly during these days and then the growth slows down, reaching the adult length around 19-25 PN days (about 22.2 m). The disks are synthesized at the base of ROS and, as new disks are formed, they progress towards the apex of the structure. The disk are discrete units, which keep the same size and the same content (meaning that proteins do not diffuse through the outer segment) [18]. As far as concerns the dark current, it roughly increases with the length of ROS [19], reaching a peak of 12pA around 20 PN days. The fact that the dark current increases with the length of ROS suggests that the density of cGMP-gated channels (that are responsible for the dark current) remains constant during the development of the retina. Since the TRP phenomenon is linked to the early stages of the transduction cascade (before hyperpolarization), the number of channels on the plasma membrane should not influence the amplitude of ROS movement.

According to Samardzija (2012) [20], the amount of bleachable rhodopsin in the wild type mouse is about 120 pmol per retina at 15 PN days and it reaches the maximal value of 550 pmol after 49 PN days. Between 15 and 28 PN days, the amount of rhodopsin grows linearly and

then, the rate of increase slows down and gradually reaches the adult level. Since the length of ROS reaches the adult value at 19-25 PN days and the amount of rhodopsin reaches the adult value at 59 PN days, the concentration of rhodopsin in ROS should be lower for younger mice [21]. Dodge et al. (1996) [22], proved this and also found out that there is a gradient in rhodopsin concentration along ROS; the older disks (which are closer to the tip of the ROS) have a lower concentration of rhodopsin since they were synthesized at a younger age. This means that, upon stimulation during the developmental age, it is more probable that rhodopsin from younger disks is bleached.

### 2.3 Stiles-Crawford effect

The sensitivity of the retina to a light stimulus depends on the incident angle of the stimulus on the retina [6; 2]. In photopic conditions, the luminous efficiency of a light beam is maximal when it enters approximately through the center of the pupil and it decreases for more peripheral positions. With their experiments, Stiles and Crawford found the equation that rules this phenomenon in the human eye:

$$\eta(d) = \eta(d_m)10^{-p(\lambda)(d-d_m)^2} \tag{2.1}$$

The relative luminance efficiency ($\eta$) depends both on the distance from the center of the pupil and the wavelength of the light beam. $d_m$ represents the gap between the center of the pupil and the point that perceives the maximum light intensity and d is the distance from that

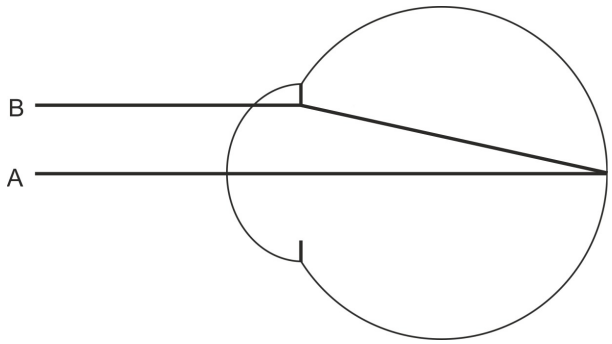


Figure 2: Two rays entering the retina at different positions have two different luminous efficiencies. Ray A is perceived as more intense by the subject even if it has the same intensity as ray B. Image adapted from [2]

point (positive towards the temporal side and negative towards the nasal side). $p(\lambda)$ is the parameter that takes into account the wavelength dependency of the phenomenon.

Photoreceptors (both rods and cones) are perpendicular to the back-side of the eyeball and they are naturally oriented towards the center of the pupil [23]. A light beam entering from the center will be parallel to the photoreceptors but, when the beam enters from a more peripheral position, it will reach them obliquely. When the pupil is dilated, the amount of light reaching the photoreceptors is considerable; the SCE reduces the sensitivity to oblique light and improves visual resolution. On the other hand, scotopic vision relies more on sensitivity rather than visual acuity. The absence of SCE in rods allows the eye to be sensitive independently from the angle of incidence of the light on the photoreceptors.

Possible causes of the SCE could involve the wave-guiding properties of cone photoreceptors, which would explain their directional sensitivity [24; 25]. However, the models are still too

simple to provide a reasonable and exhaustive explanation. The fact that rods are not involved in this phenomenon has been explained by the discovery of their phototropism (see section 2.4).

## 2.4 Transient Retinal Phototropism

TRP was first assessed in 2013 by Rongwen Lu et al., in both frog and mouse retina [8]. The study focused more extensively on frog retinae because of the easier handling of the retina and the larger size of the photoreceptors (almost 4 times larger than mouse), which allows the unambiguous identification of single rod cells. The imaging was performed through a NIR light digital microscope and the stimulation of the photoreceptors was achieved through a oblique rectangular green light. The phototropism was strongly rod dominated (an average value of $0.2\mu m$ for rods and of $0.048\mu m$ for cones in frog retina, with an active ratio of 80% and 20% respectively) and it was also directional, as the movement followed the direction of the light stimulus. The response of the photoreceptors was quick for both animals (about $10ms$ for frog and $5ms$ for mouse) therefore, it is not possible to detect it with the psycho-physical methods that are used to study the SCE. A year later, rod outer segment are identified as the mechanical source of the phototropism [26]. Optical coherence tomography combined with line-scan confocal microscopy allowed to observe the structure of the photoreceptors during the stimulation both from a cross-sectional and a frontal point of view. The cross-sectional images revealed that the movement of the rod cells was generated by the movement of the rod outer segment. A more accurate cross-sectional observation of freshly isolated frog retinae slices showed that the movement of ROS is due to an unbalanced conformational change in the disks due to rhodopsin bleaching [27; 28]. When the oblique light stimulus reaches a photoreceptor,

only the exposed part of the disk shrinks, causing a global shift towards the direction of the stimulus. When the photoreceptor is uniformly exposed to a light stimulus, both sides of the disk shrink. The fact that the disks are discrete and independent units, as they are physically separated from the cell membrane, is probably crucial to this behavior. Moreover, this can explain why cones do not exhibit phototropism when stimulated. The conformational changes of bleached rhodopsin, which is embedded in the disks membrane, could be the main reason of the shrinkage. Thanks to the registration of the electroretinogram concurrent to the classical NIR light microscopy, it was possible to understand that the phototropism occurs before the hyperpolarization of the photoreceptors [3]. This means that the physiological causes should be investigated among the early stages of the phototransduction cascade. The experiments were also repeated by replacing Ringer's solution with a low-sodium medium and this did not affect the amplitude nor the offset of the phototropism. These findings confirm that the closing of the sodium-gate channels does not play a role in phototropism.

# CHAPTER 3

# METHODS

## 3.1 Experimental setup

The experimental setup was similar to the one used in the previous studies on TRP.

In my study, there were two sets of mice, one from cage 1 and the second from cage 2. The considered PN ages were 15, 17 and 19. For each PN day, two mice from each cage were sacrificed, for a total number of 8 retinae for each PN day.

### 3.1.1 Sample preparation

The wild type mice (Mus musculus) where dark adapted at least four hours before the experiment, which was performed in dark conditions except for the presence of dim red light, in order to not elicit an unwanted response from the photoreceptors. The mouse was euthanized and both eyes were removed and stored in a dish plate containing Ringer's solution. The solution contains 110.0 $mM/L$ $NaCl$, 2.5 $mM/L$ $KCl$, 1.6 $mM/L$ $MgCl_2$, 1.0 $mM/L$ $CaCl_2$, 22.0 $mM/L$ $NaHCO_3$, and 10.0 $mM/L$ D-glucose. The eyes were hemisected and the retinae were set apart from the RPE. The isolated retinae were stored in a dish containing Ringers' solution. The mice were sacrificed one at the time in order to perform the experiment on the freshest retinae possible. The entire experiment was completed within 2 hours after the mouse was sacrificed.

For the experiment, one retina was placed on a dish with ROS facing upwards and then covered with a mesh to keep it as flat as possible. This setup allowed a clear vision of the rod photoreceptors. The retina was manually perfused with warm Ringers solution (around 37C to keep the retina in physiological conditions) about each 2-3 minutes. The dish was placed under the Near-Infrared light microscope for the imaging. All the experiments were performed following the protocols approved by the Animal Care Committee (ACC) at the University of Illinois at Chicago.

### 3.1.2 Imaging system

For the imaging system, a modified NIR light microscope (BX531WI, Olympus, Japan) was used, with a 60X water immersion objective. The light that provided the optical imaging came from a halogen lamp with a band-pass filter (wavelength range 775 to 1000 $nm$). The images were acquired through a high-speed camera (Neo 5.5, Andor Technology Ltd., Belfast, Ireland), with a pixel size of 6.5x6.5 $\mu m$. The complete setup is showed in Figure 3.

### 3.1.3 Light Stimulus

A fiber-coupled LED emitting a green light provided the stimulus (wavelength range 450 to 650 $nm$, central wavelength of 550 $nm$). The green visible light differs from the red one used for image acquisition because this wavelength elicits the movement of the photoreceptors. The sensitivity of mouse rod photoreceptors is maximum for the green-blue wavelength. The light was tilted in order to elicit a shift of the photoreceptors and observe the directionality of the phenomenon; it was coming from upward with an angle of roughly 30 degrees, as shown in Figure 4. The size of the light stimulus was controlled through an adjustable slit. The

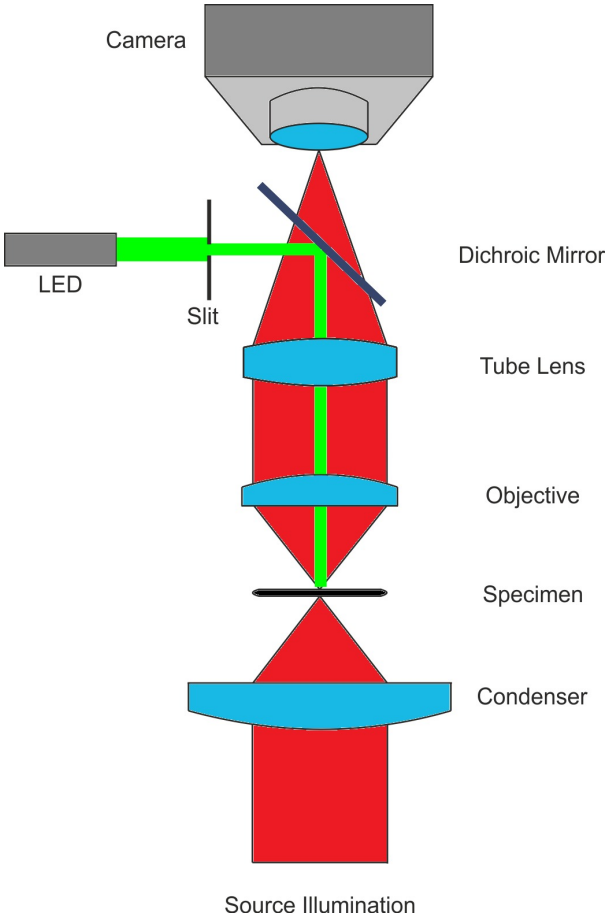


Figure 3: Experimental setup used for the imaging of the retina. Image adapted from [3].

rectangular light stimulus covered about one fourth of the central part of the acquisition window and the light flash lasted for one second. On the retina, the width of light stimulus was about $15\mu m$, which is enough to cover multiple photoreceptors (which have a diameter of about $2\mu m$). Figure 5 shows the image of the retina with the limits of the light stimulus; it is possible to observe the imaged photoreceptors.

The stimulus intensity was roughly $1.0 \cdot 10^8 photon/\mu m^2 \cdot s$, which is enough to elicit a consistent movement of the photoreceptors. The experiments were performed on a floating table in order to cancel any noise vibration that may affect the photoreceptors.

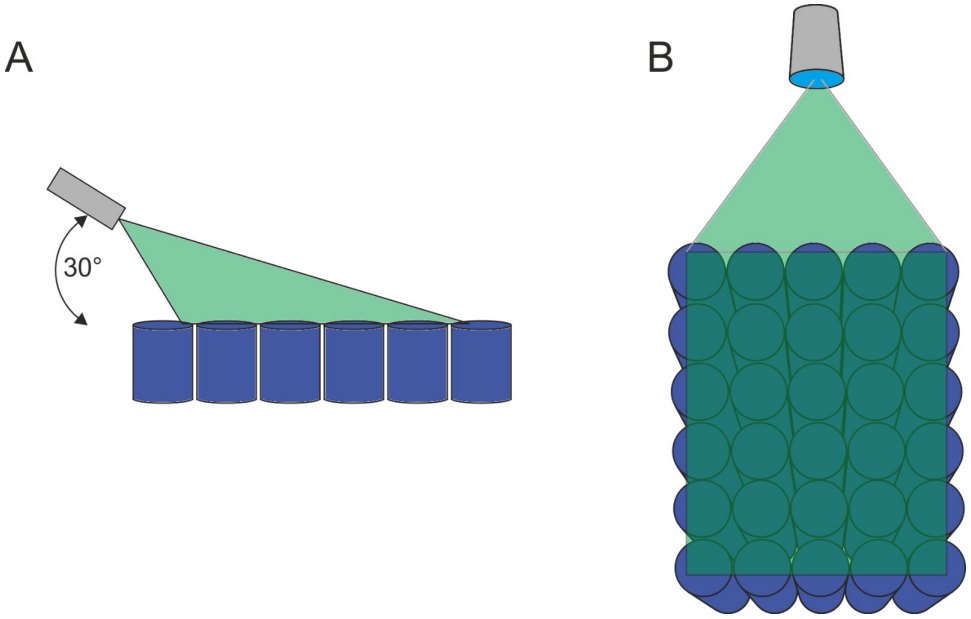


Figure 4: Direction of the stimulus with respect of the ROS. Image A shows a side view of the retina; with this representation it is possible to observe the incident angle of the light stimulus on the photoreceptors. The stimulus angle is relative to the normal direction. In image B it is possible to see the frontal view, which is the actual view at which the images were acquired.

### 3.1.4 Image sequence

The features of the image sequence are the following:

- Acquisition window: 512x512 pixels
- Number of images: 400
- Frame rate: 100fps
- Acquisition time: 4s
- Stimulus start: 1s
- Stimulus duration: 1s
- The stimulus starts at frame 100 and ends at frame 200.

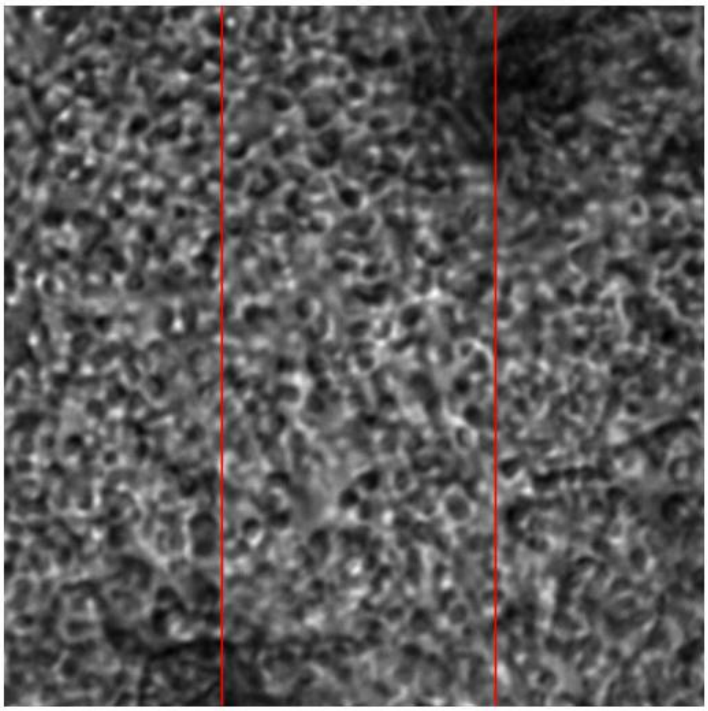

Figure 5: Image acquired during the experiments. The red lines show the limits of the light stimulus on the retina. The stimulus covers multiple photoreceptors; some of them are clearly distinguishable.

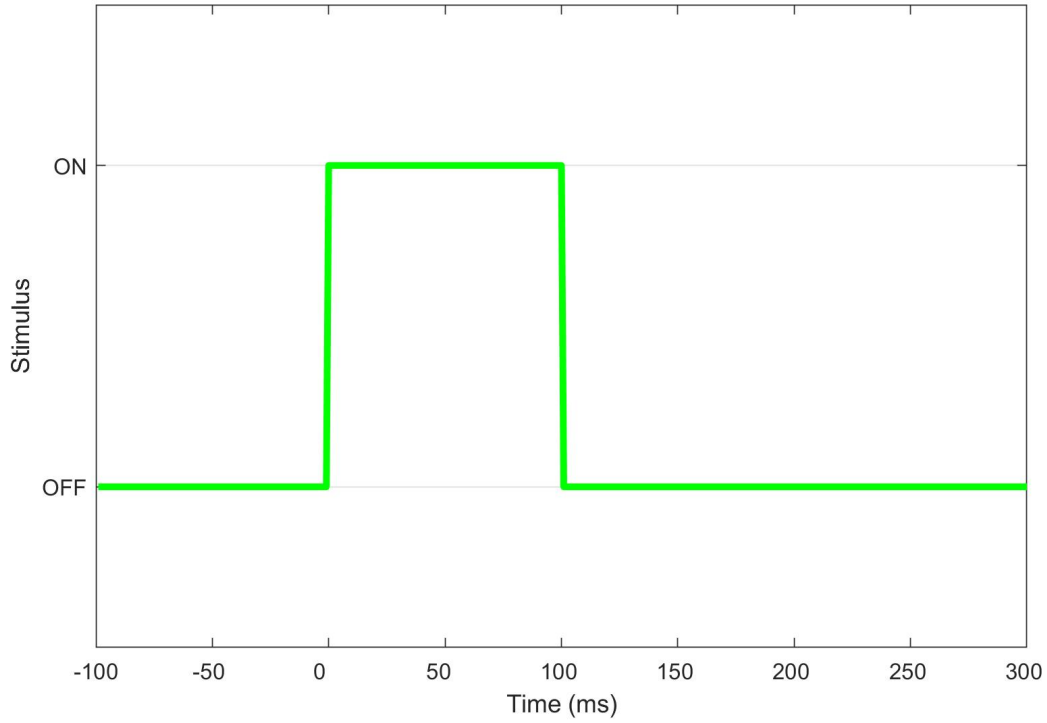


Figure 6: Duration of the stimulus. The stimulus starts at frame 100, which is considered as time zero, and it lasts up to 1s. Each second covers 100 frames.

### 3.2 Data Processing

The Optical Flow Algorithm developed by Sun et al . was used to process the images [29]. The algorithm allows to compare two images of a sequence and to quantify the movement between the two. This makes it suitable to track the motion of ROS between the non-stimulated and the stimulated images. The images were cropped in order to analyze the movement only in the stimulated area and also to reduce the computing time. To provide the amplitude of ROS movement, each frame in the sequence was compared to a reference one (frame 85), which was not stimulated. In order to have a general idea of the behavior of the photoreceptors, the average movement in the stimulated area for each frame was computed. This method is not precise as far as concerns the actual shift of the single photoreceptors but it allows to understand their global behaviour and to neglect or at least to reduce the contribution of movements that were not elicited by the light stimulation. For example, in some image sequences there was a vibration of the photoreceptors regardless the stimulation or there were corpuscles floating in the imaged area.

# CHAPTER 4

# RESULTS

## 4.1 Data Analysis

The response of the photoreceptors to the light stimulus was visible during the image acquisition phase. There was a clear difference between 15 PN days and the older retinae; the motion of the photoreceptors became stronger and more clear. Two mice from the same cage were analyzed on the same day of experiments, meaning that each set of samples comes from 4 different retinae. The following table (Table I) shows the number of image sequences acquired for each group. In some cases one of the retinae was not completely healthy and it was not possible to observe the photoreceptors. Those retinae were discarded so, in that case, the images were acquired from three retinae instead of four. From a single retina, 5 to 10 image sequences were acquired.

TABLE I: NUMBER OF SAMPLES FOR EACH GROUP

| | **15 PN Days** | **17 PN Days** | **19 PN Days** |
|---|---|---|---|
| **Cage 1** | 25 | 28 | 33 |
| **Cage 2** | 35 | 23 | 17 |

### 4.1.1 Amplitude

The average movement at each PN day for each frame is computed. In this is way it is possible to have a first understanding of the differences between the three ages.

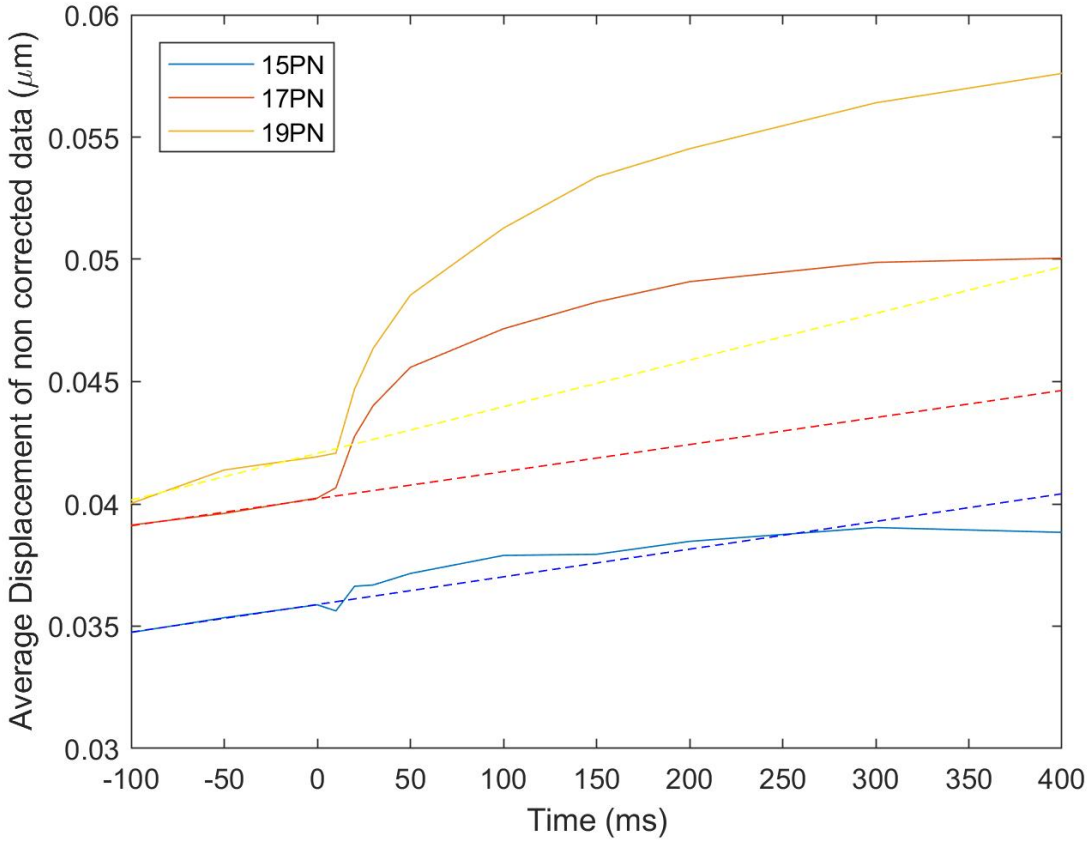


Figure 7: Mean of the average movement in the stimulated area for each analyzed PN day. The dashed line is the computed regression line.

It is possible to observe that there is a movement of the photoreceptors even before the stimulation. There are two main explanations for this. First, there is a slow and constant shift of the photoreceptors that was not completely removed with the image registration and second, in some cases I observed a random vibration of the photoreceptors that added a constant contribution to the average movement (this second contribution does not affect the shape of the curve but it adds a offset). The drift will affect the final results, causing an overestimation of the real values of the movement. For this reason, I decided to quantify this drift and remove it from the original values (I assumed that the drift had a constant slope). The dashed lines in Figure 7 represent the estimated drift for each group. The lines were computed by calculating linear regression of the values at the first three frames. The assumption behind this choice is that there should be no movement before the stimulation, hence the first three points should lie on the same horizontal line. Once the drift is removed, the values are shifted in order to have the movement at frame 100 at the zero level. In this way it is easier to compare the movement at different PN ages. The next figure (Figure 8) shows the average movement at each frame with the corrected values (the drift is removed).

With this representation, the values of the movement are more coherent with literature values, even though they are still higher. Moreover, it is easier to compare the three ages and to observe the motion elicited by the light stimulus. The difference between the three curves is clear between 15 PN days and the other two ages. The phototropism reaches its peak after 100ms for 15PN days and around 200ms for 17 and 19 PN days.

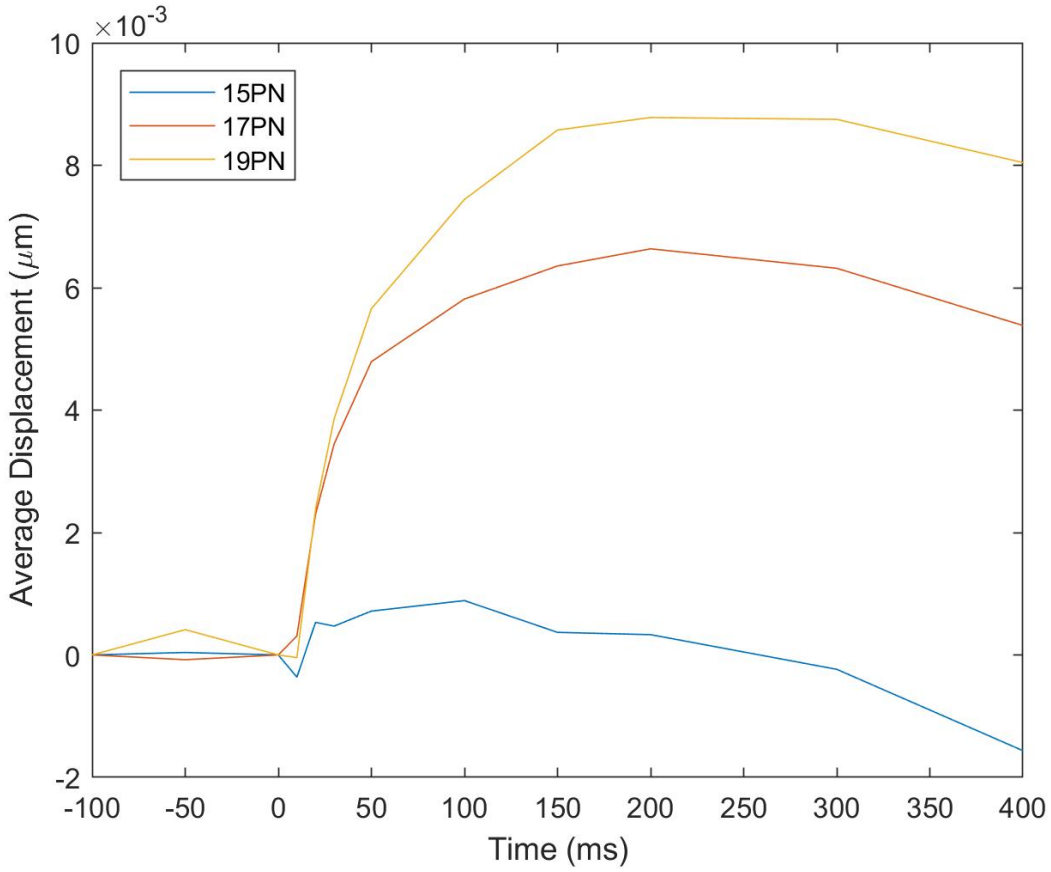


Figure 8: Comparison of the average movement of the photoreceptors at each PN day with drift correction applied.

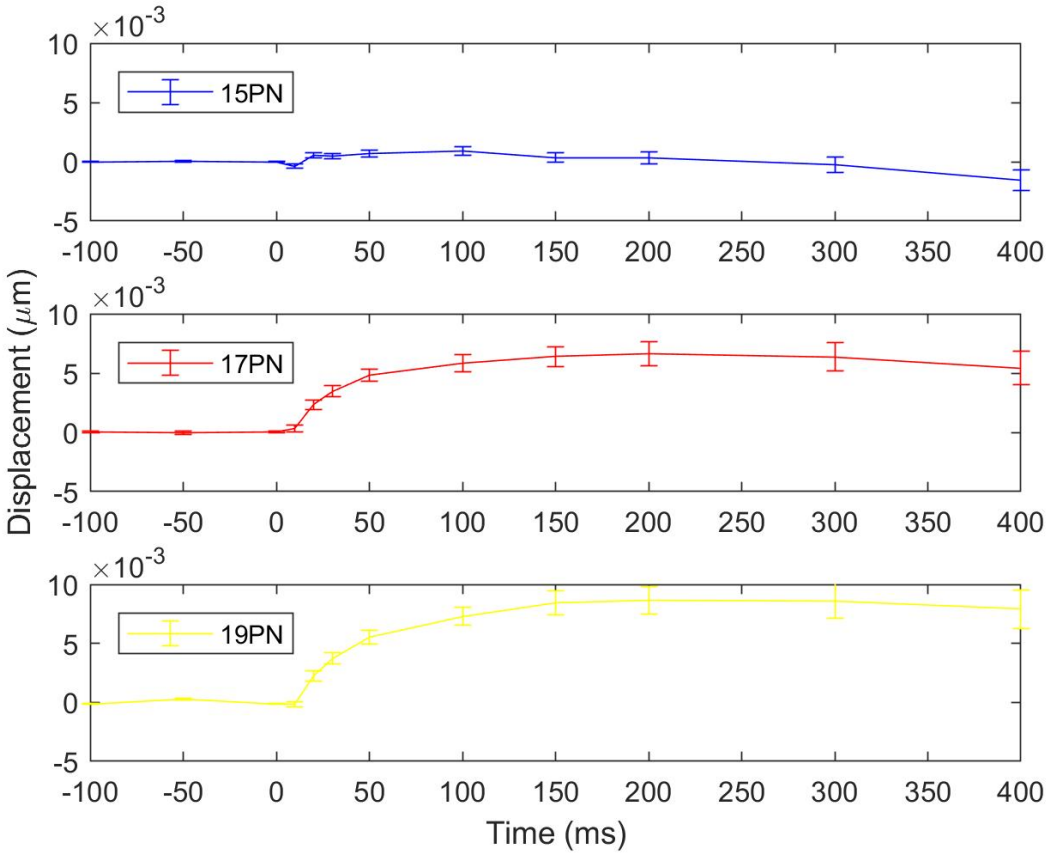


Figure 9: Average shift of the photoreceptors each PN Day with standard errors.

The average amplitude increases with the post-natal days of the mice. The boxplot reports the maximum shift value of the average movement for each image sequence. It is possible to observe that the major difference is between 15 PN days and 17 PN days (the average value is more than 3 times higher). These values are obtained after the removal of the drift and their order of magnitude is smaller than literature values. This may depend on the fact that I analyzed the mean movement in the stimulated area instead of focusing on the movement of single ROS. Table II reports the mean values with the standard errors of the drift corrected samples and Figure 10 shows a plot of the values. The standard errors are computed according to the formula:

$$se = \frac{\sigma}{\sqrt{n}} \tag{4.1}$$

in which $\sigma$ represents the standard deviation and n represents the number of samples.

TABLE II: AVERAGE MAXIMUM SHIFT FOR EACH PN DAY WITH STANDARD ERRORS. VALUES WITH DRIFT CORRECTION

| | **15 PN Days** | **17 PN Days** | **19 PN Days** |
|---|---|---|---|
| **Mean** | 0.0026 | 0.0088 | 0.0105 |
| **Std Error** | $\pm$0.0003 | $\pm$0.0008 | $\pm$0.0011 |

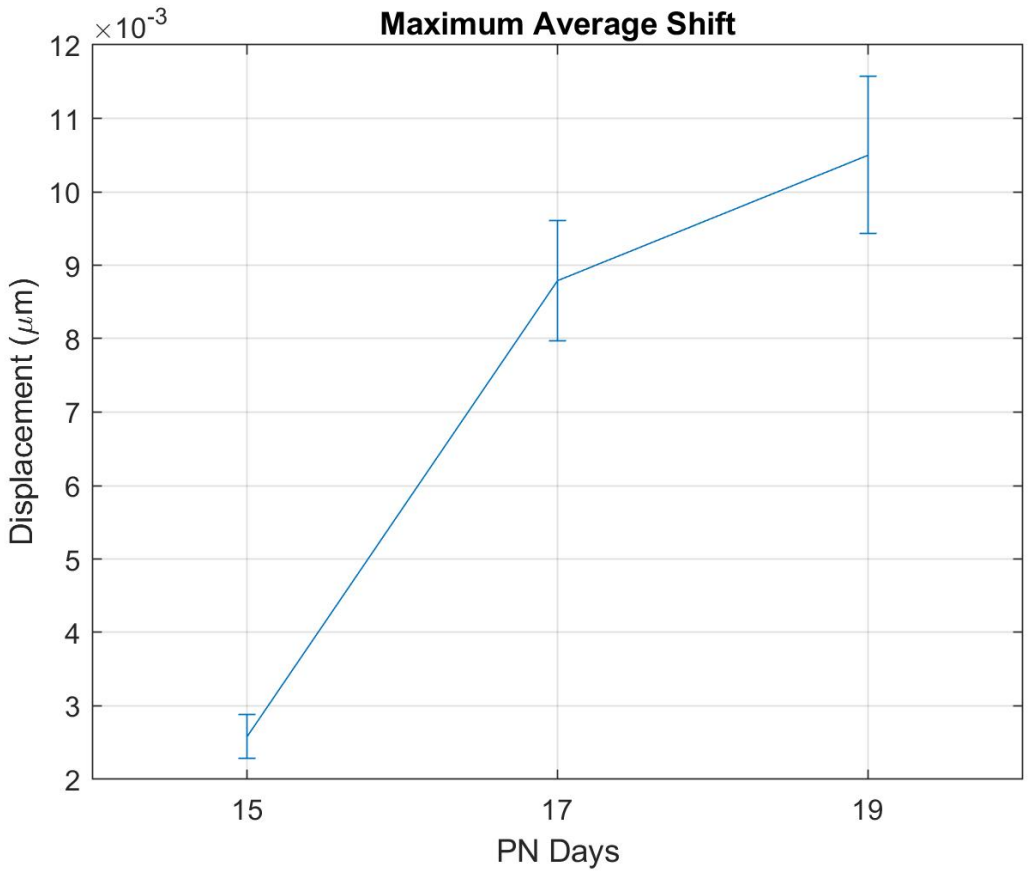


Figure 10: Maximum of the average drift-corrected shift for each PN day. The error bars represent the standard error.

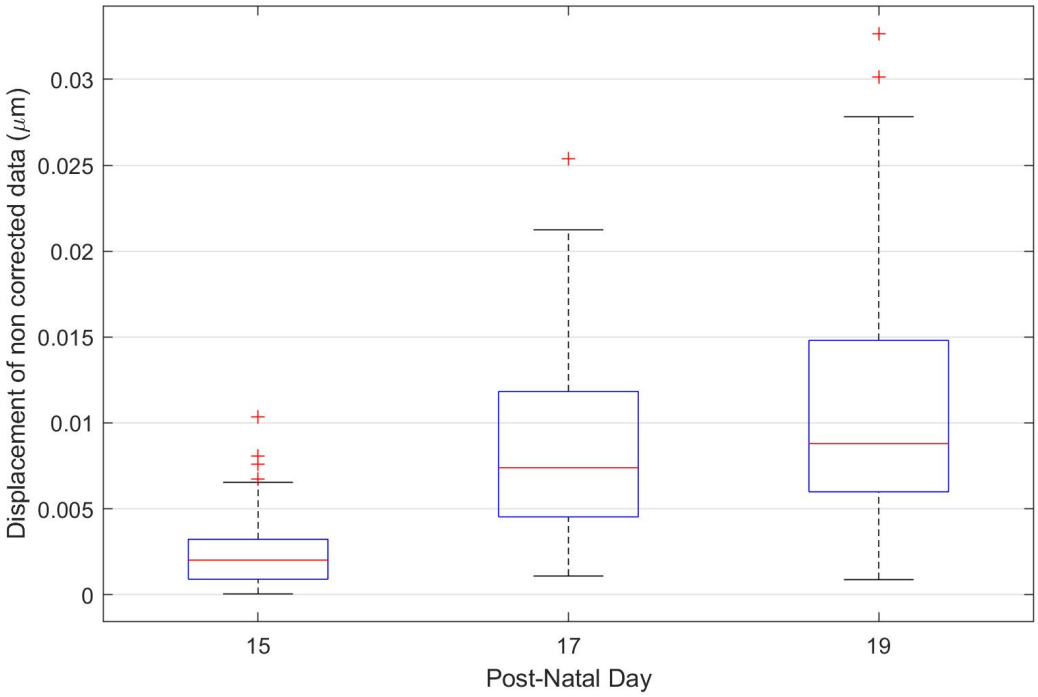


Figure 11: Boxplot with the maximum movements for each PN day.

As far as concerns the onset of the stimulation, there are no significant changes in the different post-natal days. The onset is between 10 and 20 milliseconds for each post-natal day. Anyway, since the images are acquired at 100 fps, it could be possible that the difference in the onset is smaller than 10ms and so, it is not possible to detect it with this temporal resolution. Figure 12 shows the amplitude of phototropism in the five frames following the stimulation.

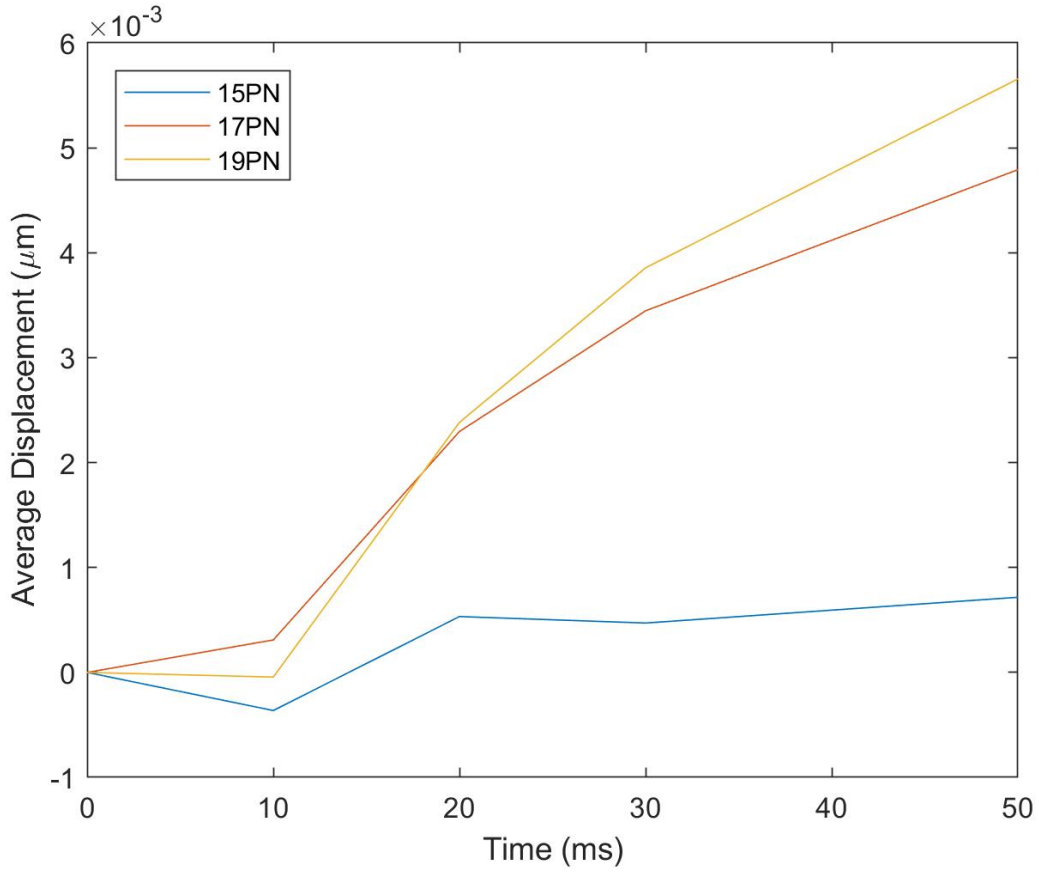


Figure 12: Average movement of ROS with zoom on the first milliseconds after the light stimulation.

Another observation on the response of ROS is that the movement of the photoreceptors was not completely restricted to the stimulation area. Since the retina is really small, it is probable that the movement of the stimulated photoreceptors also affects the adjacent ones, causing a movement outside the stimulated area. However, since the images are cropped to the stimulated area only, this kind of behavior is not involved in the results.

### 4.1.2 Direction of the movement

In order to analyze the angles of the responses for each PN day, I removed the offset from the data and then the three sigma rule was used to extract only the angles related to the active movement. Since the light stimulus is coming from upwards, I decided to analyze the number of responses that have a direction angle between 45 and 135 degrees.

The thresholding of the active areas is performed by computing an amplitude threshold based on the mean and the standard deviation of the values in the non-stimulated frames. For each pixel the threshold is set at the mean value plus three times the standard deviation. In this way, a matrix of threshold values is created and used to distinguish the active areas from the movement due to the noise. Figure 13 shows the active areas (white pixels) of one image sequence (17 PN days) after the application of the three sigma rule for each frame of the sequence.

In the following figure (Figure 14) are also reported the histograms of the active angles for each stimulated frame for the same image sequence. The black lines delimit the values that are considered as upwards movement. The x axis shows the angle values (from -180 to 180 degrees). In this example there is a strong phototropic response of the photoreceptors.

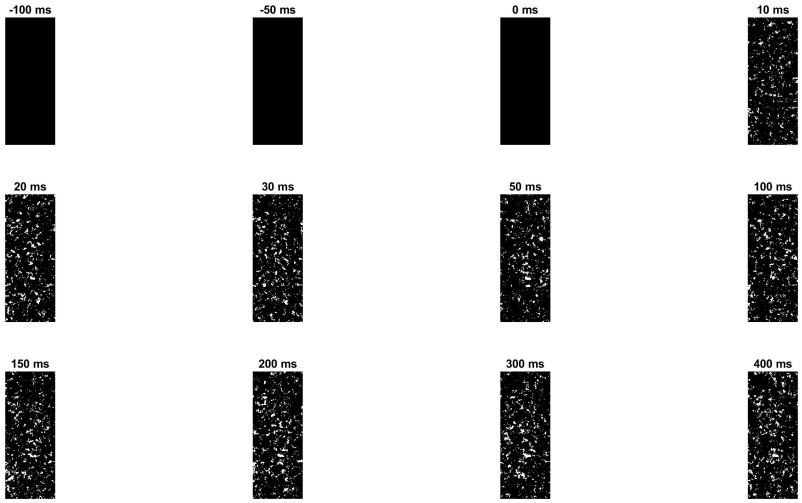


Figure 13: Active areas after thresholding with the three-sigma rule

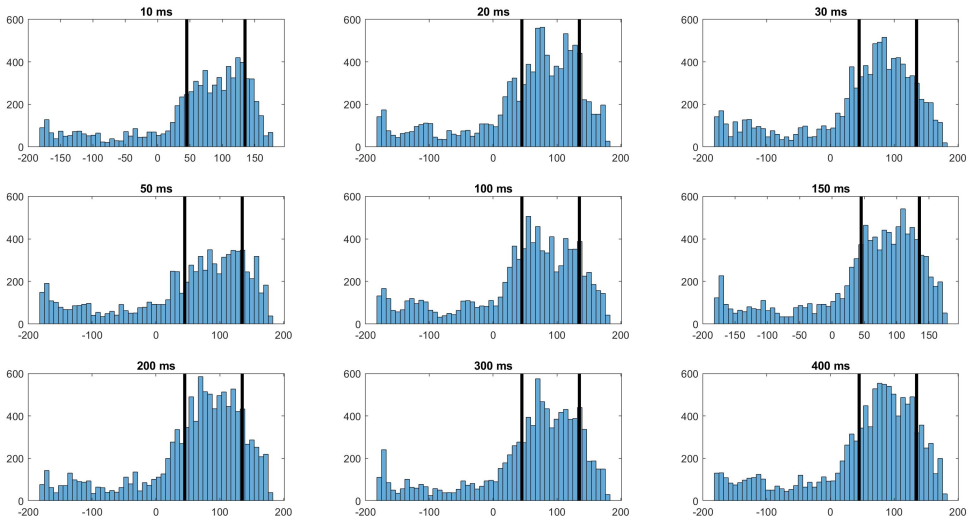


Figure 14: Histograms of the angles of the active areas for each analyzed frame. The black lines delimit the angles that are considered upwards.

For the analysis of the angles, I decided to focus on one frame of the sequence, in particular I decided to use frame number seven (50 ms after the stimulation) for the analysis. For each PN day and each image sequence I extracted the response at 50 ms and I analyzed the angles of the motion in the active areas only. The angles were divided in upwards direction (45 to 135 degrees) and other directions. Then, the percentage of angles moving upwards was calculated for each image sequence. Table III and Table IV show the median and the interquartile range of the results for each cage at each PN day.

TABLE III: MEDIAN VALUES OF THE PERCENTAGES OF ANGLES MOVING UPWARDS FOR EACH CAGE AND EACH PN DAY

| | **15 PN Days** | **17 PN Days** | **19 PN Days** |
|---|---|---|---|
| **Cage 1** | 23,45% | 31,12% | 31,24% |
| **Cage 2** | 29,03% | 26,44% | 27,47% |

TABLE IV: INTER-QUARTILE RANGE VALUES OF THE PERCENTAGES OF ANGLES MOVING UPWARDS FOR EACH CAGE AND EACH PN DAY

| | **15 PN Days** | **17 PN Days** | **19 PN Days** |
|---|---|---|---|
| **Cage 1** | 9,98% | 12,94% | 18,99% |
| **Cage 2** | 12,45% | 28,15% | 15,50% |

Since the range of degrees considered covers one fourth of the total range, in a random situation, the percentage of angle moving upwards should be around 25%. Since the movement is phototropic, hence it follows the direction of the stimulus, the percentages should be higher than 25%. It is interesting to observe how the percentage increases between 15 PN days and the other two ages.

The following histogram (Figure 15) shows the distribution of the percentages for each PN day. The red line represents the 25% reference. The black line is the median of the distribution. In the case of 17 and 19 PN days, the median is greater than 25%, which means that the movement is responding to the light stimulus with a slightly phototropic response. On the other hand, the 15 PN day distribution does not show a predominant movement in the upward direction.

In order to have a better comprehension of the distribution, I decided to analyze the number of image sequences that exhibits a percentage higher than 25%. This value is not influenced by the outliers and gives a better index to understand the behavior of the movement. Table V shows the percentages of image sequences with a ratio of angles going in the upwards direction higher than 25%. In the second line the total number of image sequences for each PN day is showed. Figure 16 shows which image sequences exceed the 25% threshold. The red dashed line is at 25% and the blue crosses are the percentages that are higher than the threshold.

It is really interesting to observe how the number of responses that are higher than 25% significantly increases between 15 and 17 PN days. This number will probably be even higher in the adult mouse. At 15 PN days not even half of the responses can be considered phototropic.

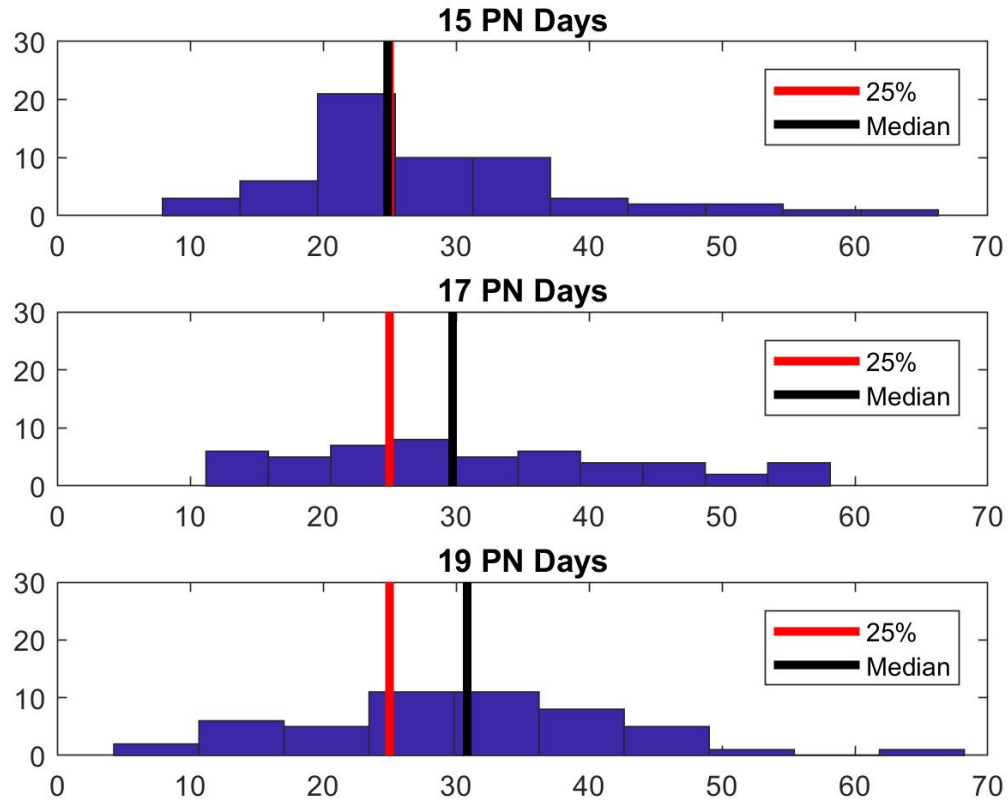


Figure 15: Histograms of the angles of the active areas for each analyzed frame. The black lines delimit the angles that are considered upwards.

TABLE V: PERCENTAGES OF IMAGE SEQUENCES THAT SHOWED A PHOTOTROPIC RESPONSE TO THE LIGHT STIMULUS

| | **15 PN Days** | **17 PN Days** | **19 PN Days** |
|---|---|---|---|
| **Percentage** | 49,15% | 64,71% | 66,00% |
| **Number of sequences** | 59 | 51 | 50 |

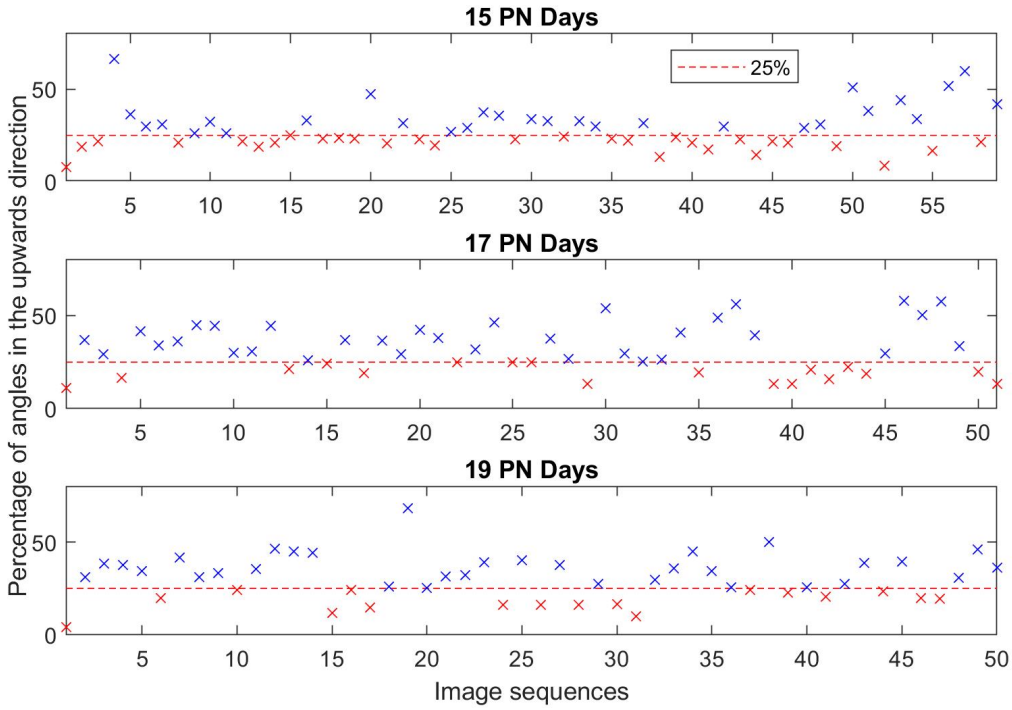


Figure 16: Plot of the percentages of angles moving upwards for each image sequence. Each cross represents the value for a image sequence. The blue crosses represent the value that are greater than the 25% threshold and the red crosses represent the values that are smaller. The dashed red line is the 25% reference.

As the photoreceptors grow and the rhodopsin concentration increases, the response of the cells is less random and more often towards the light stimulus. This could be due to the fact that a higher concentration of rhodopsin translates to a higher probability that the photosensitive molecules on the stimulated side will bleach and cause the movement of the photoreceptor.

The fact that the percentages are still low could be related to the in vitro conditions of the experiment. The behavior of the photoreceptors in vivo is probably different and it would exhibit higher percentages of photoreceptors moving in the direction of the stimulus. Also, a higher inclination of the light stimulus should be able to elicit a stronger directional response.

## 4.2 Statistical Analysis

### 4.2.1 Protocol

The statistical analysis is performed to test the normality of the data, the connection between the two cages and the differences between the three PN ages.

Since each sample reaches its peak at different frames, the variable taken in consideration for this statistical analysis is the maximum amplitude of the mean movement of the stimulated area. The values were collected in six different arrays, one for each cage and for each PN age.

TABLE VI: NUMBER OF SAMPLES FOR EACH GROUP

| | **15 PN Days** | **17 PN Days** | **19 PN Days** |
|---|---|---|---|
| **Cage 1** | 25 | 28 | 33 |
| **Cage 2** | 35 | 23 | 17 |

However, since the data do not come from different retinae but for each retina there are different samples, the values are averaged in order to obtain a single value for each retina. The number of samples is greatly reduced, but each value is an average of 5-10 samples. The new arrays have the length showed in Table VII.

TABLE VII: NUMBER OF SAMPLES FOR EACH GROUP AFTER RETINA AVERAGING

| | **15 PN Days** | **17 PN Days** | **19 PN Days** |
|---|---|---|---|
| **Cage 1** | 3 | 4 | 4 |
| **Cage 2** | 4 | 3 | 3 |

The first test performed is the Kolmogorov-Smirnov test for normality. This test assumes as null hypothesis that the data are normally distributed. The six distributions are tested separately. The result determines whether parametric or non-parametric tests can be used on the data.

In the first test, the data from the two cages are assumed coming from different distributions and so, they are tested separately. This assumption is checked with the Wilcoxon rank sum test (or MannWhitneyWilcoxon test), a non-parametric test, which assumes as null hypothesis that two independent samples follows the same continuous distribution (with the same medians). The outcome of this test reveals if the data from the two cages (for the same PN age) can be seen as a single distribution. In case that the test accepts the null hypothesis, it is possible to

legitimately see them as a unique array, increasing the number of samples and allowing a more robust analysis.

The next step is the Kruskal-Wallis test. It is similar to the Wilcoxon rank sum but it can inspect more than two populations at the time. In this way, we can test the samples coming from the three different ages and understand if there is a statistical difference between them. Afterwards, it will be necessary to perform a *post hoc* analysis in order to see which ages can be seen as statistically different, since the test reveals only if there is a dissimilarity between at least two groups. This test is performed twice, first on the three distributions of cage number one and then on the three distributions of cage number two.

For each test, the significance level is set at 5%. The analysis was performed on both the drift corrected and the original data. For the non-corrected data, the values where shifted so that the movement amplitude at frame 100 (at which the light stimulus is applied) is zero, moreover the considered frame interval for the identification of the maximum is 100-120. In this way it is possible to compare the different samples regardless their movement before the stimulation and the attention is on the 200 ms after the stimulation, in which the peak of the phototropism should be reached. Since the offset removal applied to the 15 PN days data lead to negative values, the absolute value was computed.

### 4.2.2 Results of the original dataset

First of all, let us observe the distribution of the maximum shift for the original values. The considered interval to compute the maximum is between frame 101 and 120, in this time window the movement elicited by the light stimulus should have reached its peak and the movement

generated by an eventual image drift is limited. The complete equation used to compute the maximum shift is reported in Equation 4.2.

$$y = \left| \max_{[101,120]} (shift) - shift(100) \right| \tag{4.2}$$

Figure 17 shows the distributions of the samples before the average per retina is computed. With this representation, it is possible to have a better understanding of the dispersion of the values. Figure 18 shows the same variable once the values are averaged. The low sample size makes it harder to have a clear idea of general behavior but this figure represents the distribution of the arrays that will actually be used for the statistical analysis.

By the histograms of the data, it is possible to observe that none of the groups seems to be normally distributed but this is strongly affected by the limited number of observations. Let us observe the boxplot of the different distributions in Figure 19. The main difference seems to be between 15 and 17 PN days, whereas the increase between 17 and 19 PN days seems limited. The values are overlapped and there is not a clear difference between the two ages. It is possible that as this age, the values are already saturating at the adult ones. The Kruskal-Wallis test will reveal if there is a statistically significant increase between the two ages.

The Kolmogorov-Smirnov test was performed on each one of the six vectors and for all of them, the null hypothesis was not rejected. However, the test is not reliable because of the low sample size; the test cannot reject the null hypothesis because of the low n and not because of the real distribution of the data. The resulting p-values are showed in Table VIII.

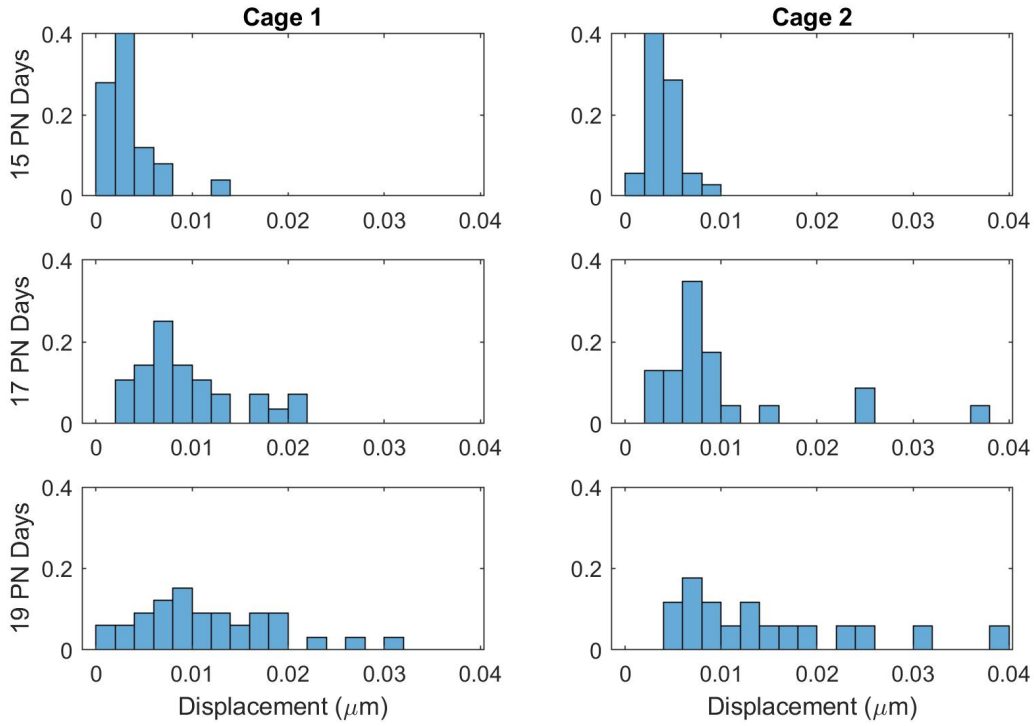


Figure 17: Frequency of the maximum average movement for the non-corrected data. The shift is expressed in micrometers.

As far as concerns the Wilcoxon rank sum test, for each age, the null hypothesis was not rejected. This means that the data coming from the two cages can be merged, forming three arrays (one for each PN age) instead of six. This almost doubles the number of samples for each distribution, leading to a more reliable result. Again, the low number of samples interferes with the result of the test but the merge of the two cages is crucial to have a significant statistical analysis. The table displays the p-values for each PN day.

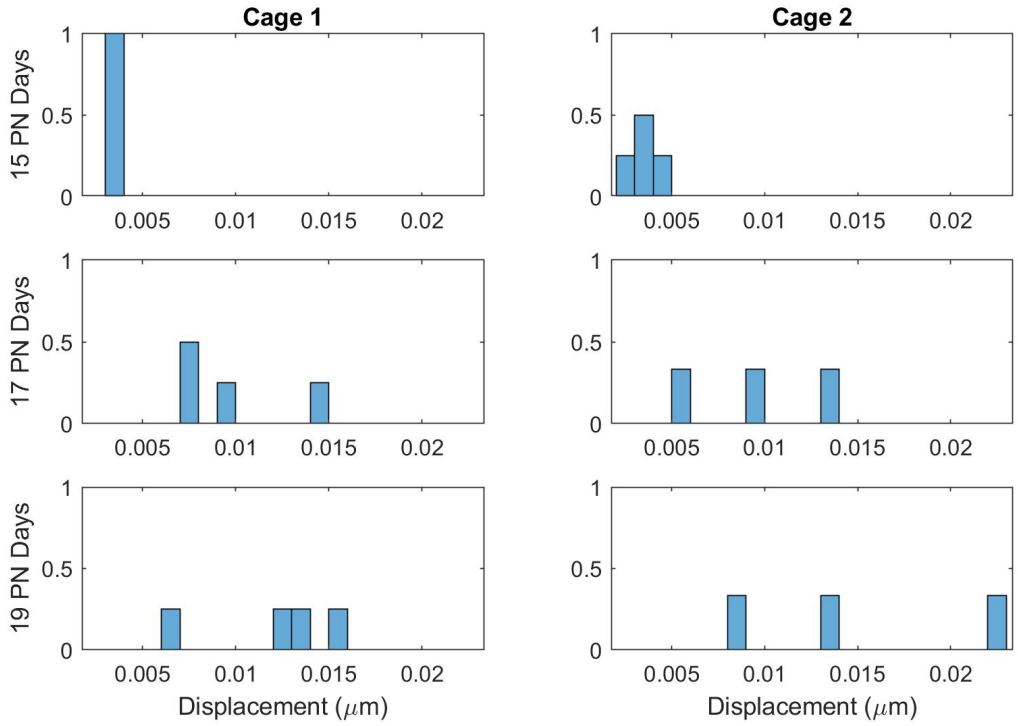


Figure 18: Frequency of the maximum average movement for the non-corrected data. The shift is expressed in micrometers.

The normality of the values is checked again with the Kolmogorov-Smirnov test and, in this case, the null hypothesis can be rejected for each PN day (Table X), this shows that the data do not follow a normal distribution and the previous result was determined by the lower sample size.

The distribution of the variable for the unified cage is shown in Figure 20. Again, the main difference is between 15 and 17 PN days.

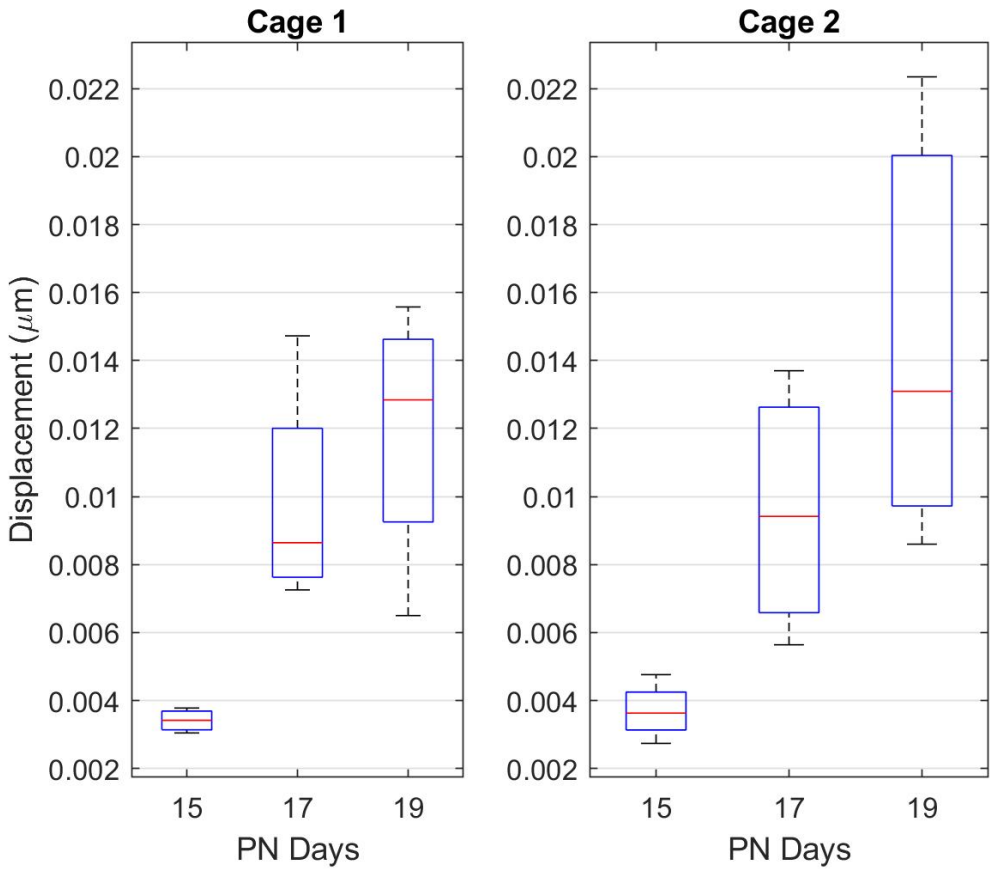


Figure 19: Boxplots showing the distribution of the maximum average shift for each PN day. The shift is expressed in micrometers.

The data is finally tested with Kruskal-Wallis and the resulting p-value is approximately $9.5872e-04$. It is possible to reject the null hypothesis and assert that there is a significant difference between the means of the three PN ages. In order to exploit this result and understand which groups are different, it is necessary to perform the *post hoc* analysis. The output of the

TABLE VIII: P-VALUES OF THE KOLMOGOROV-SMIRNOV TEST ON THE NON-CORRECTED DATA

| | **15 PN Days** | **17 PN Days** | **19 PN Days** |
|---|---|---|---|
| **Cage 1** | 0.3305 | 0.1828 | 0.1833 |
| **Cage 2** | 0.1857 | 0.3281 | 0.3254 |

TABLE IX: P-VALUES OF THE WILCOXONRANK-SUM TEST ON THE NON-CORRECTED DATA

| | **15 PN Days** | **17 PN Days** | **19 PN Days** |
|---|---|---|---|
| **P-Value** | 0.8571 | 1 | 0.8571 |

multiple comparison test confirmed that there is a significant difference between the data from 15 PN days and the other two groups but this is not true between 17 and 19 PN days.

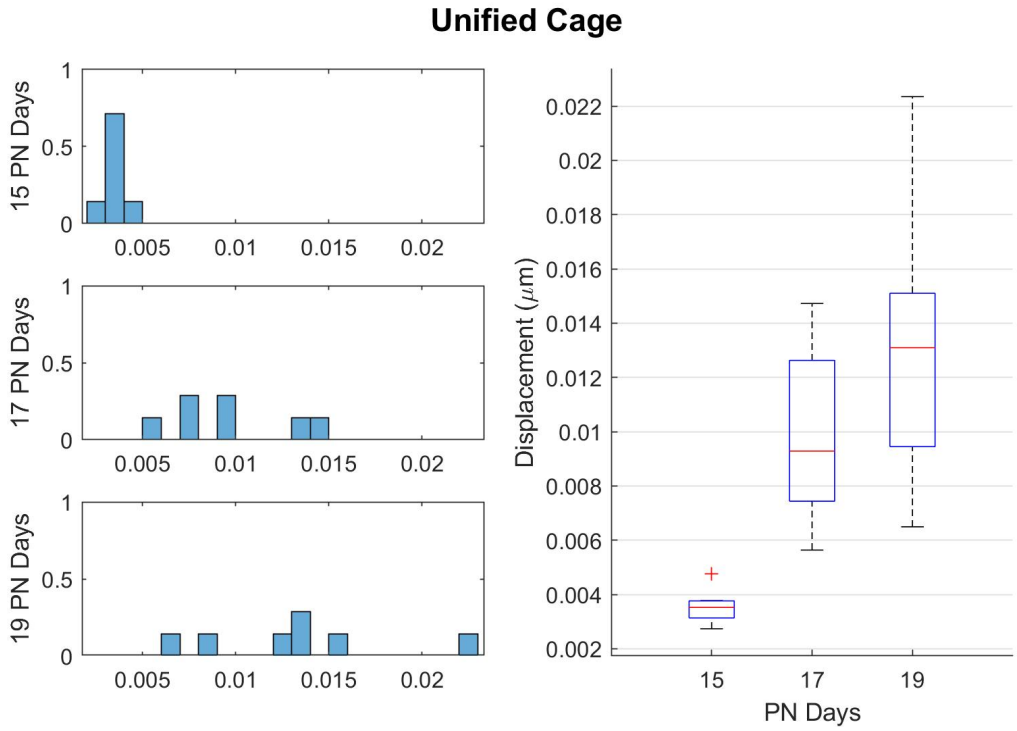


Figure 20: Boxplots and histograms of the maximum shift for the unified cage. The shift is expressed in micrometers.

TABLE X: P-VALUES OF THE KOLMOGOROV-SMIRNOV TEST ON THE NON-CORRECTED DATA, WITH UNIFIED CAGES

| | **15 PN Days** | **17 PN Days** | **19 PN Days** |
|---|---|---|---|
| **P-Value** | 0.0377 | 0.0370 | 0.0368 |

### 4.2.3 Results of the drift-corrected dataset

The same protocol is now applied to the dataset with the drift correction. In this case, the considered time interval goes from frame 101 to frame 120. The drift correction is applied assuming that the values frame interval 90-100 should be horizontally aligned since there is no stimulation. The parameters of the line are computed through a linear regression applied in that frame interval. Finally, the regression line is removed from the original data and the maximum value of the average movement is calculated as difference with the amplitude value at frame 100 (see Equation 4.2). The distribution of the variable for the six different groups is as showed in Figure 21. Then, the average for each retina is computed leading to the distribution showed in Figure 22.

It is observable that the difference between 17 and 19 PN days is really subtle in this dataset. The distributions for these days in both cages seem to overlap and the difference between the means are smaller than the non-corrected dataset. The boxplots also show the same behavior (Figure 23), in the second cage the mean value at 19 PN days is smaller than 17 PN days. This means that the Kruskal-Wallis test will not find a statistical difference between the distribution at these ages. Again, The Kolmogorov-Smirnov test did not reject the null hypothesis but this result is due to the low number of samples rather than statistical evidence. The p-values are shown in Table XI.

The Wilcoxon Rank Sum test reveals that the two cages can be attributed to the same distribution for the three ages. The result is surely affected by the limited sample size but the merge of the cages will help the outcome of the analysis.

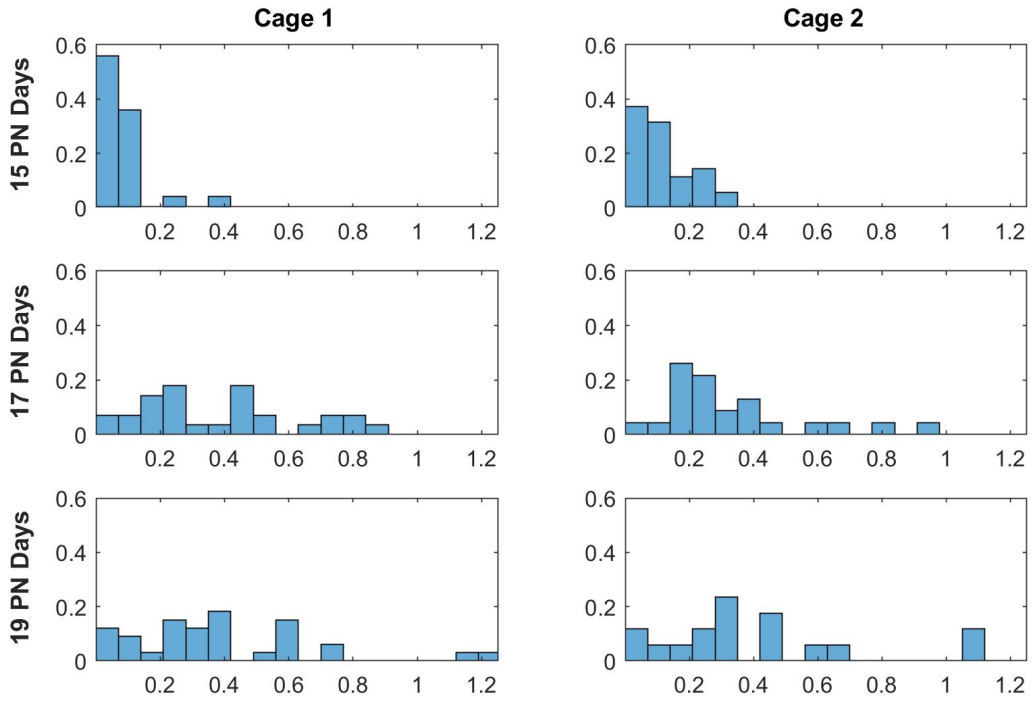


Figure 21: Frequency of the maximum average movement for the non-corrected data. The shift is expressed in micrometers.

It is more clear from the boxplot in Figure 24, representing the unified cage distribution, that the data from 17 and 19 PN days are similar and they overlap for the most of the values. The data are not normally distributed according to the Kolmogorov-Smirnov test with a 5% significance level.

The Kruskal-Wallis test return a p-value equal to 0.0012. This means that the null hypothesis is rejected and so there are statistically significant differences between the two distributions.

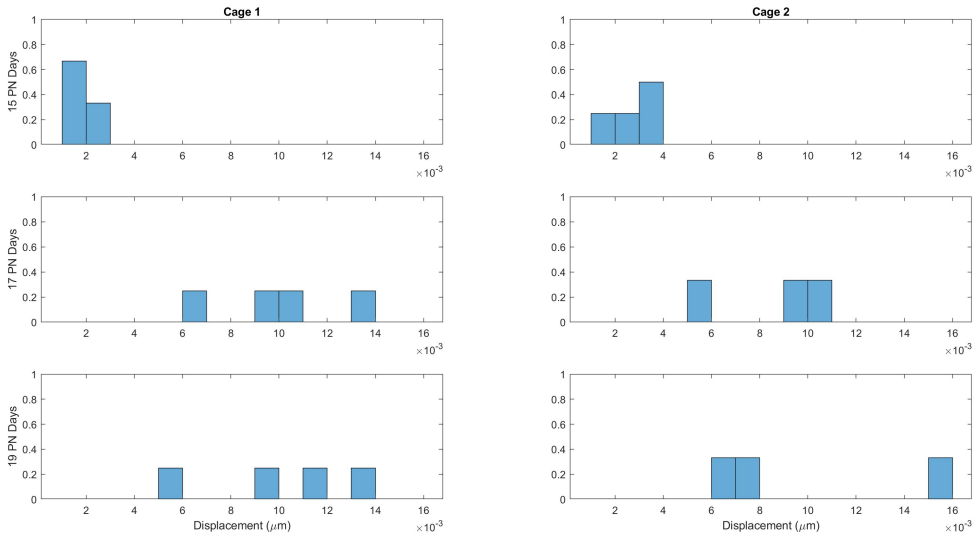


Figure 22: Frequency of the maximum average movement for the non-corrected data. The values are computed by averaging the multiple values of each retina. The shift is expressed in micrometers.

The multiple comparison reveals that the difference is between the data from 15 PN days and the other two ages. There is no significant difference between 17 and 19 PN days.

### 4.2.4 Discussion of the statistical analysis

Both the original and the drift-corrected datasets gave similar results. The fact that the data are not normally distributed may depend on the fact that there were not enough samples to show this kind of behavior. The Kolmogorov-Smirnov test with the separated cages does not prove that the data are normally distributed because of the lack of samples. As a matter of facts, the null hypothesis is rejected when the test is repeated with the unified data set.

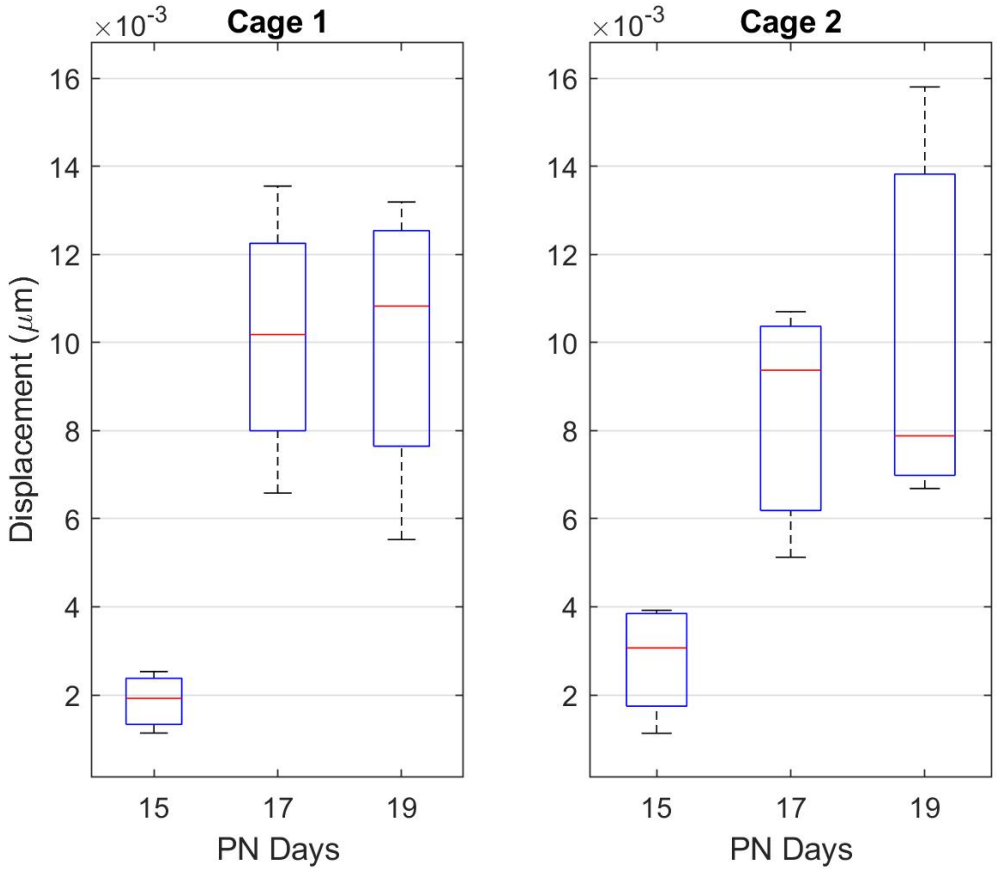


Figure 23: Boxplots showing the distribution of the maximum average shift for each PN day. The shift is expressed in micrometers.

The analysis also showed that the drift correction does not alter the statistical behavior of the data.

The results of the Kruskal-Wallis tests and its post hoc analysis are consistent with what we expected. The main difference is between 15 and 17 PN days, in which the rate of developments of the rod outer segments reaches a peak. At 17 and 19 PN days, the value is already saturating

TABLE XI: P-VALUES OF THE KOLMOGOROV-SMIRNOV TEST ON THE DRIFT-CORRECTED DATA

| | **15 PN Days** | **17 PN Days** | **19 PN Days** |
|---|---|---|---|
| **Cage 1** | 0.3323 | 0.1833 | 0.1839 |
| **Cage 2** | 0.1868 | 0.3286 | 0.3271 |

TABLE XII: P-VALUES OF THE WILCOXON RANK-SUM TEST ON THE DRIFT-CORRECTED DATA

| | **15 PN Days** | **17 PN Days** | **19 PN Days** |
|---|---|---|---|
| **P-Value** | 0.6286 | 0.4 | 1 |

to the adult one, meaning that the difference between the two ages is minimal and not significantly different. Moreover, the examined mice were visibly strong, especially the samples from cage number 2. This means that they might have developed slightly faster than the average rate.

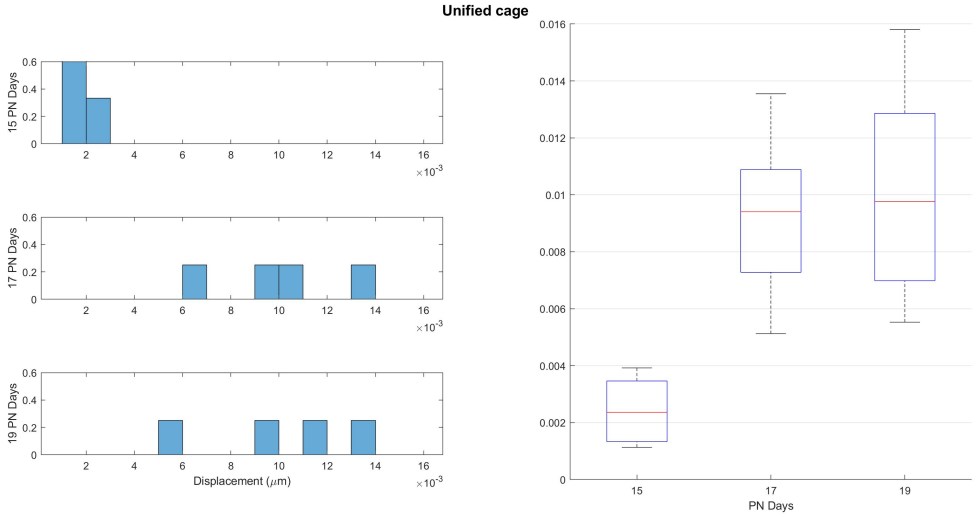


Figure 24: Boxplots and histograms of the maximum shift for the unified cage. The shift is expressed in micrometers.

TABLE XIII: P-VALUES OF THE KOLMOGOROV-SMIRNOV TEST ON THE DRIFT-CORRECTED DATA, WITH UNIFIED CAGES

| | **15 PN Days** | **17 PN Days** | **19 PN Days** |
|---|---|---|---|
| **P-Value** | 0.0381 | 0.0371 | 0.0370 |

# CHAPTER 5

# DISCUSSION

In order to explain the increase in the amplitude of phototropism between 15 and 19 PN days, it is necessary to take into account how ROS are developing in this age period. In particular, the focus of this dissertation is to explain the steeper increase observed between 15 and 17 PN days. I have taken into account different variables that increase in the 15-19 PN days range. They are fundamental in ROS development. These variables are: ROS length, content of rhodopsin per retina and dark current. The diameter of ROS remains almost constant during the growth of ROS, so the exposed surface of ROS depends only on its length. Both ROS length and the amplitude of the dark current increase linearly between 15 and 17 PN days and they reach the adult level around 19-25 PN days. This trend is the same of the amplitude of the phototropism, which has a steeper increase between 15 and 17 PN days and then a smaller growth between 17 and 19 PN days, which can mean that it is reaching the adult value (but this is only an assumption). On the other hand, the amount of rhodopsin increases linearly in this period.

The increase of rhodopsin itself cannot explain the steeper increase in the phototropism amplitude between 15 and 17 PN days. It is necessary to take into account also the fact that the photoreceptors reach a peak in their growth during the same age. The fact that the photoreceptors are longer probably affects the amplitude of the phototropism. Moreover, considering that disks closer to the base of ROS have a higher concentration of rhodopsin,

it is more probable that the rhodopsin contained in those disks will be bleached from the light stimulus. This means that the phototropism involves the shrinkage of lower disks and this results in a greater shift of the tip of the outer segment. The different amplitude in the response of ROS could also depend on different mechanical properties of the mouse retina during the developmental ages.

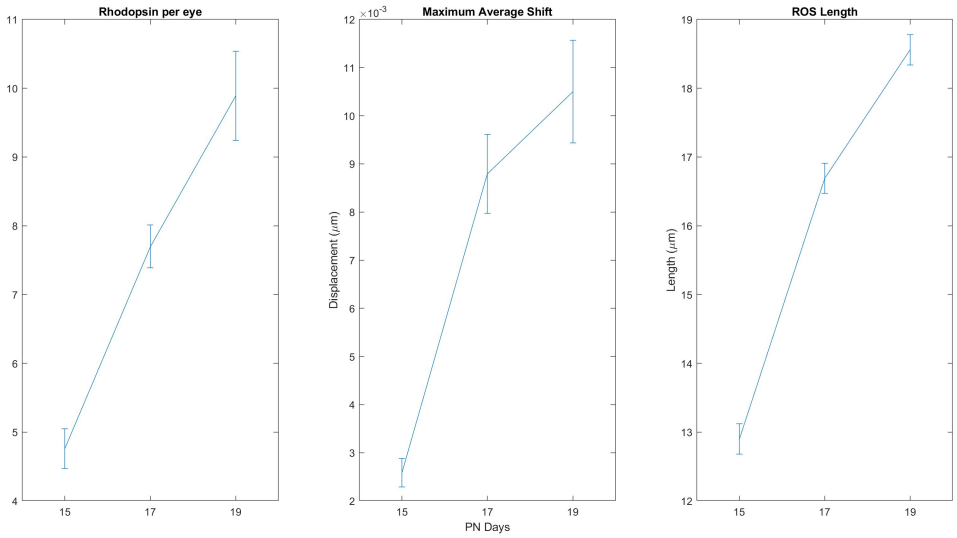


Figure 25: Growth of the different variables in the considered period of age. Maximum average movement and ROS length are both expressed in micrometers. The data for the rhodopsin per eye content comes from Caravaggio and Bonting (1963) [4]. The values were collected from averagely 16 eyes for each day. The ROS length graphic is based on the data from La Vail (1973) [5]. The value of the standard mean error was not reported for all data but the average value of 0.22 was stated. The number of samples was averagely 80.

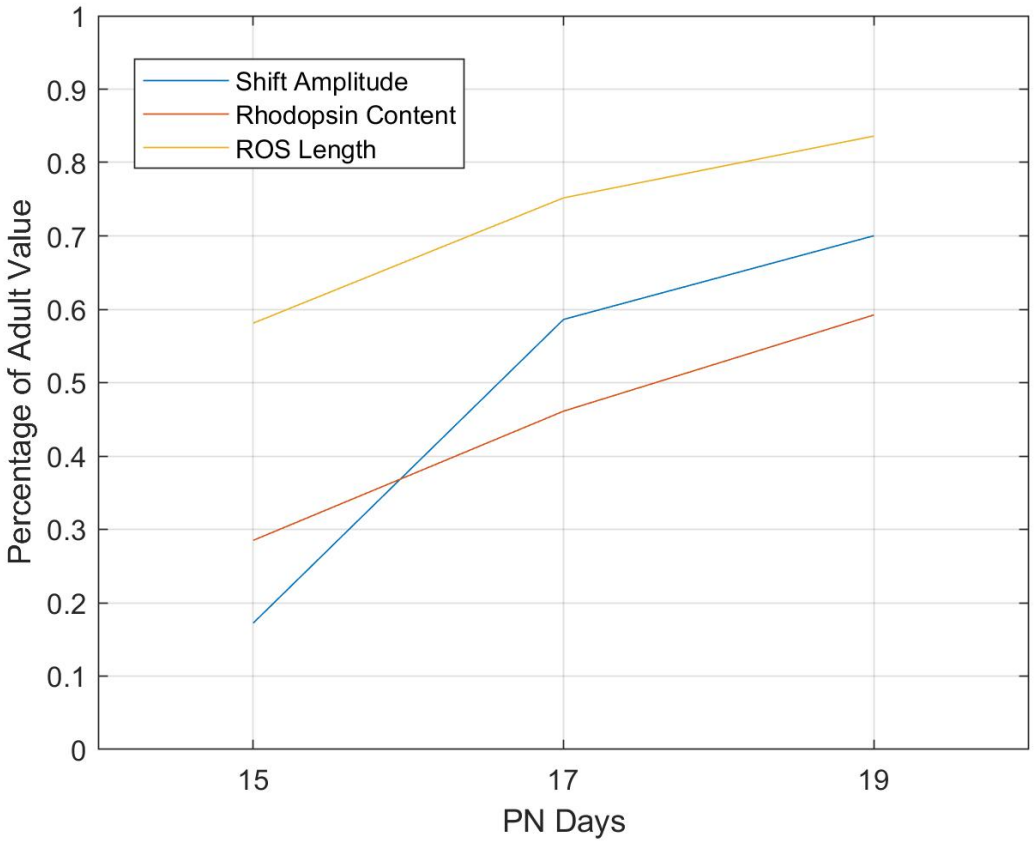


Figure 26: Increase of the different variables expressed as percentage of the adult value. The dark current is not taken into account in this graph because it follows a trend very similar to the length of ROS. The blue line represents the amplitude of the phototropism. The adult value is just an assumption for this variable as my data is only available up to 19 PN days.

# CHAPTER 6

# CONCLUSION

The rapid increase of the TRP between 15 and 17 PN ages is consistent with the fact that the major variables are quickly increasing during the same age. The bleaching of rhodopsin upon light stimulation is the more probable source of the movement. Rhodopsin is a fundamental molecule in the physiology of rod cells and it plays a key role in the development of ROS [9; 14; 30]. Therefore, further studies on the role of this molecule in phototropism could lead to interesting results.

This study was performed on freshly isolated retinae, for which it is easier to observe the tip of the photoreceptors clearly, since they are separated from the RPE and they face the camera. For a better evaluation of the TRP, *in vivo* studies of the phenomenon would be incredibly helpful. The movement of the photoreceptors could differ in the amplitude and in the onset when the retina is in its natural conditions. Moreover, it would be possible to measure the phenomenon as a function of the position of the stimulus.

Recent studies on Adaptive Optics (AO), allowed the *in vivo* observation of both cone and rod photoreceptors in the human retina [31; 32; 33]. This technology could eventually allow the assessment and quantification of phototropism in the human retina, providing a non-invasive biomarker for the early detection of retinal degeneration.

## CITED LITERATURE


1. Kolb Helga: How the retina works. American Scientist, 91:28–35, 2003.

2. Westheimer, G.: Directional sensitivity of the retina: 75 Years of Stiles-Crawford effect. Proceedings of the Royal Society B: Biological Sciences, 275(1653):2777–2786, 2008.

3. Lu, Y., Wang, B., Pepperberg, D. R., and Yao, X.: Stimulus-evoked outer segment changes occur before the hyperpolarization of retinal photoreceptors. Biomedical Optics Express, 8(1):38, 2016.

4. Caravaggio, L. L. and Bonting, S. L.: The rhodopsin cycle in the developing vertebrate retina. Experimental Eye Research, 2(1):12–19, jan 1963.

5. LaVail, M.: Kinetics of rod outer segment renewal in the rat retina. The Journal of cell biology, 58:650–661, 1973.

6. Stiles, W. S. and Crawford, B. H.: The luminous efficiency of rays entering the eye pupil at Different Points . Royal Society, 112(778):428–450, 1933.

7. Flamant, F. and Stiles, W. S.: The directional and spectral sensitivities of the retinal rods to adapting fields of different wave-lengths. The Journal of Physiology, 107(2):187–202, mar 1948.

8. Lu, R., Yao, X., Levy, A. M., Pittler, S. J., and Zhang, Q.: Dynamic near-infrared imaging reveals transient phototropic change in retinal rod photoreceptors. Journal of Biomedical Optics, 18(10):106013, 2013.

9. Rakshit, T. and Park, P. S.: Impact of Reduced Rhodopsin Expression on the Structure of Rod Outer Segment Disc Membranes. Biochemistry, 54(18):2885–2894, may 2015.

10. Curcio, C. A., Medeiros, N. E., and Millican, C. L.: Photoreceptor loss in age-related macular degeneration. Investigative ophthalmology & visual science, 37(7):1236–49, 1996.

## CITED LITERATURE (continued)


11. Lee, E. S. and Flannery, J. G.: Transport of Truncated Rhodopsin and Its Effects on Rod Function and Degeneration. Investigative Ophthalmology & Visual Science, 48(6):2868–76, 2007.

12. Hamel, C. P.: Cone rod dystrophies. Orphanet Journal of Rare Diseases, 2(1):7, dec 2007.

13. Fu, Y. and Yau, K.-W.: Phototransduction in mouse rods and cones. Pflugers Archiv : European journal of physiology, 454(5):805–19, aug 2007.

14. Palczewski, K.: G ProteinCoupled Receptor Rhodopsin. Annual Review of Biochemistry, 75(1):743–767, jun 2006.

15. Baylor, D. A., Lamb, T. D., and Yau, K. W.: Responses of retinal rods to single photons. The Journal of physiology, 288:613–34, mar 1979.

16. Young, R. W.: THE RENEWAL OF PROTEIN IN RETINAL RODS AND CONES. The Journal of Cell Biology, 39(1):169–184, oct 1968.

17. Young, R. W. and Bok, D.: Participation of the retinal pigment epithelium in the rod outer segment renewal process. The Journal of cell biology, 42(2):392–403, aug 1969.

18. Young, R. W.: The renewal of photoreceptor cell outer segments. The Journal of Cell Biology, 33(1):61–72, 1967.

19. Luo, D.-G. and Yau, K.-W.: Rod Sensitivity of Neonatal Mouse and Rat. The Journal of General Physiology, 126(3):263–269, sep 2005.

20. Samardzija, M., Wariwoda, H., Imsand, C., Huber, P., Heynen, S. R., Gubler, A., and Grimm, C.: Activation of survival pathways in the degenerating retina of rd10 mice. Experimental Eye Research, 99(1):17–26, 2012.

21. Fulton, A. B., Hansen, R. M., and Findl, O.: The development of the rod photoresponse from dark-adapted rats. Investigative Ophthalmology and Visual Science, 36(6):1038–1045, 1995.

22. Dodge, J., Fulton, A. B., Parker, C., Hansen, R. M., and Williams, T. P.: Rhodopsin in immature rod outer segments. Investigative Ophthalmology and Visual Science, 37(10):1951–1956, 1996.

## CITED LITERATURE (continued)


23. Laties, A. M. and Enoch, J. M.: An analysis of retinal receptor orientation. Investigative Ophthalmology & Visual Science, 10:69–77, 1971.

24. Snyder, A. W. and Pask, C.: The Stiles-Crawford effectexplanation and consequences. Vision Research, 13(6):1115–1137, jun 1973.

25. Vohnsen, B., Iglesias, I., and Artal, P.: Guided light and diffraction model of human-eye photoreceptors. Journal of the Optical Society of America. A, Optics, image science, and vision, 22(11):2318–28, nov 2005.

26. Wang, B., Zhang, Q., Lu, R., Zhi, Y., and Yao, X.: Functional optical coherence tomography reveals transient phototropic change of photoreceptor outer segments. Optics Letters, 39(24):6923, dec 2014.

27. Zhao, X., Thapa, D., Wang, B., Gai, S., and Yao, X.: Biophysical mechanism of transient retinal phototropism in rod photoreceptors. Optical Interactions with Tissue and Cells XXVII, 9706, mar 2016.

28. Zhao, X., Thapa, D., Wang, B., Lu, Y., Gai, S., and Yao, X.: Stimulus-evoked outer segment changes in rod photoreceptors. Journal of Biomedical Optics, 21(6):065006, jun 2016.

29. Sun, D., Roth, S., and Black, M. J.: Secrets of optical flow estimation and their principles. In 2010 IEEE Computer Society Conference on Computer Vision and Pattern Recognition, pages 2432–2439. IEEE, jun 2010.

30. Lem, J., Krasnoperova, N. V., Calvert, P. D., Kosaras, B., Cameron, D. A., Nicolo, M., Makino, C. L., and Sidman, R. L.: Morphological, physiological, and biochemical changes in rhodopsin knockout mice. Proceedings of the National Academy of Sciences, 96(2):736, 1999.

31. Roorda, A., Romero-Borja, F., Donnelly III, W. J., Queener, H., Hebert, T. J., and Campbell, M. C.: Adaptive optics scanning laser ophthalmoscopy. Optics Express, 10(9):405–412, may 2002.

32. Dubra, A., Sulai, Y., Norris, J. L., Cooper, R. F., Dubis, A. M., Williams, D. R., and Carroll, J.: Noninvasive imaging of the human rod photoreceptor mosaic using a confocal adaptive optics scanning ophthalmoscope. Biomedical Optics Express, 2(7):1864, jul 2011.

## CITED LITERATURE (continued)

33. Merino, D., Duncan, J. L., Tiruveedhula, P., and Roorda, A.: Observation of cone and rod photoreceptors in normal subjects and patients using a new generation adaptive optics scanning laser ophthalmoscope. Biomedical Optics Express, 2(8):2189, aug 2011.

34. Jan, L. Y.: ULTRASTRUCTURAL LOCALIZATION OF RHODOPSIN IN THE VERTEBRATE RETINA. The Journal of Cell Biology, 62(2):257–273, aug 1974.

35. Olney, J. W.: An electron microscopic study of synapse formation, receptor outer segment development, and other aspects of developing mouse retina. Investigative Ophthalmology & Visual Science, 7(3):250–268, 1968.

36. Reuter, T.: Fifty years of dark adaptation 1961-2011. Vision Research, 51(21-22):2243–2262, 2011.

# VITA

| | |
|---|---|
| NAME | Vittoria Maneo |
| EDUCATION | B.S., Biomedical Engineering, Sep 2016, Polytechnic of Milan, Italy |
| LANGUAGE SKILLS | |
| Italian | Native speaker |
| English | Full working proficiency |
| | 2013 - IELTS examination (27.0/9) |
| | A.Y. 2017/18 One Semester of study abroad in Chicago, Illinois |
| SOFTWARE AND PROGRAMMING LANGUAGES | |
| | Experience with Excel and MATLAB |
| | Basic knowledge in C |
| WORK EXPERIENCE AND PROJECTS | |
| March 2016 - June 2016 | Participation on the development of a Cortical Magnetic Stimulator prototype for cortical mapping. The work was performed with other two bachelor students and two master students at NearLab, Polytechnic of Milan. |
| Summer 2018 | Work experience in a gym (Movimenti, Germignaga, Italy). My tasks were primarily involving data analysis and creating effective reports to improve the management. On the side, I am still teaching Hip-hop to kids and adults. |